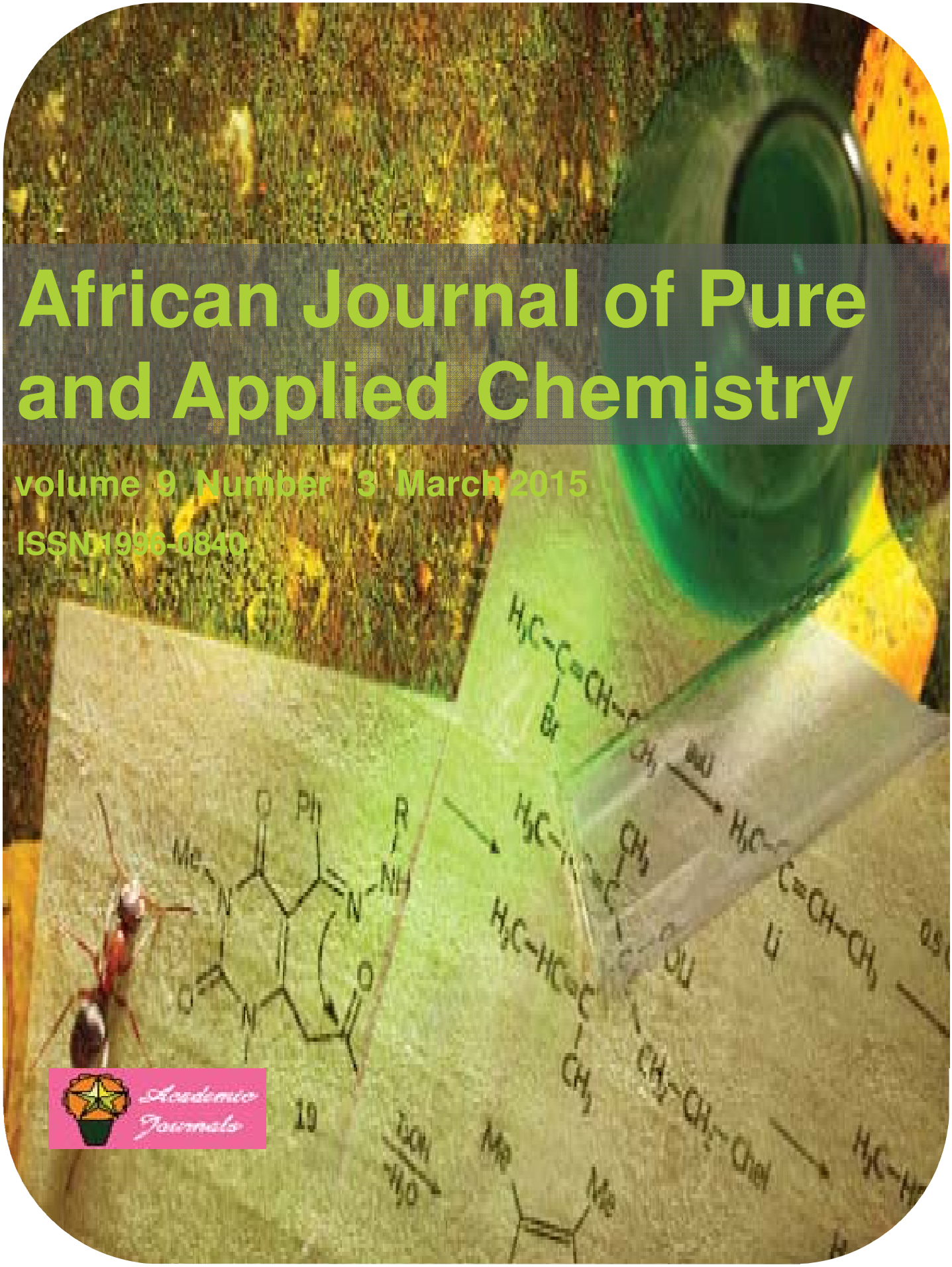

African Journal of Pure and Applied Chemistry

volume 9 Number 3 March 2015

ISSN 1996-0840

ABOUT AJPAC

The **African Journal of Pure and Applied Chemistry (AJPAC)** is an open access journal that publishes research analysis and inquiry into issues of importance to the science community. Articles in AJPAC examine emerging trends and concerns in the areas of theoretical chemistry (quantum chemistry), supramolecular and macromolecular chemistry, relationships between chemistry and environment, and chemicals and medicine, organometallic compounds and complexes, chemical synthesis and properties, chemicals and biological matters, polymer synthesis and properties, nanomaterials and nanosystems, electrochemistry and biosensors, chemistry and industry, chemistry and biomaterials, advances in chemical analysis, instrumentation, speciation, bioavailability. The goal of AJPAC is to broaden the knowledge of scientists and academicians by promoting free access and provide valuable insight to chemistry-related information, research and ideas. AJPAC is a bimonthly publication and all articles are peer-reviewed.

African Journal of Pure and Applied Chemistry (AJPAC) is published twice a month (one volume per year) by Academic Journals.

Contact Us

Editorial Office: ajpac@academicjournals.org

Help Desk: helpdesk@academicjournals.org

Website: http://www.academicjournals.org/journal/AJPAC

Submit manuscript online http://ms.academicjournals.me/.

Editors

Editorial Board

African Journal of Pure and Applied Chemistry

Table of Contents: Volume 9 Number 3 March, 2015

ARTICLES

Research Articles

academicJournals

Vol. 9(3), pp. 33-38, March, 2015
DOI: 10.5897/AJPAC2015.0615
Article Number: 663EF5F51544
ISSN 1996 - 0840

http://www.academicjournals.org/AJPAC

African Journal of Pure and Applied Chemistry

Full Length Research Paper

Physiochemical characterisation and level of potentially toxic metals in surface water around yauri abattoir, north western Nigeria

Yahaya M. I.[1]* and Agbendeh Z. M.[2]

[1]Department of Chemistry, Sokoto State University, Sokoto State, Nigeria.
[2]Department of Applied Chemistry, Federal University Dutsin-Ma, Katsina State, Nigeria.

Received 6 February, 2015; Accepted 9 March, 2015

Physicochemical and potentially toxic metals statuses of surface water samples collected around the Yauri abattoir were examined. Health risk assessment of the toxicant via ingestion was interpreted by calculating the hazard quotient (HQ). The mean concentration values for total dissolved solid (TDS), total suspended solid (TSS), dissolved oxygen (DO), phosphate, and biochemical oxygen demand (BOD) were 1026.78, 565.22, 5.0, 8.89 and 484.64 mg/L respectively. The values are above those obtained for the control water sample as well as those of international safe limits for water. The values of pH (6.6), sulphate (86.91 mg/L), nitrate (41.45 mg/L) and chemical oxygen demand (COD) (903.30 mg/L) fell within world health organization maximum permissible limits for drinking water. The mean concentrations of Co (6.93 mg/L), Cu (14.45 mg/L), Fe (64.16 mg/L), and Zn (37.14 mg/L) were above both the control and WHO, EU and EPA safe limits for metals in water. On the other hand Cd (11.47 mg/L), Ni (35.49 mg/L), and Pb (41.94 mg/L) had a mean concentration values which are higher than the international standard limits and control water sample. The calculated values of HQ show that Cd, Co, Cu and Ni were of high risk, Fe with a medium and Pb and Zn are of low risk. Correlation coefficients revealed general positive and significant correlations between the pairs of metals in water. The results of this study showed some levels of pollution of the stream water indicating that the activities at the abattoir were contributing to the pollution load of water in the area.

Key words: Yauri, abattoir, toxic metals, physicochemical.

INTRODUCTION

Pollution of the environment by toxic metals even at low levels and their resulting long term cumulative health effects are among the leading health concerns all over the world. They are non-biodegradable, thus persisting for long periods in environmental ecosystems. Environmental pollution has generally become a threat to the existence of humanity and the ecosystem. Some pollution effects may lead to metabolic disorders and undesirable changes which in many cases cause severe injuries and health hazards (Alorge, 1992).

Abattoir can be defined as a premise approved and registered by controlling authorities for hygienic

*Corresponding author. E-mail: ymansur64@gmail.com

slaughtering, inspection, processing, effective preservation and storage of meat products for human consumption. However, meat processing activities in Nigeria are generally carried out in unsuitable buildings and by untrained staff or butchers who are most of the time unaware of sanitary principles (Olanike, 2002).

Abattoir activities may be another source of pollution since human activities such as animal production and meat processing have been reported to influence negatively on soil and natural water composition leading to pollution of the soil, natural water resources and the entire environment (Adesemoye et al., 2006). Activities at the abattoir are aimed at optimizing the recovery of edible portions of the meat processing cycle for human consumption. However, significant quantities of secondary waste materials are also generated during this process. For example, blood, fat, organic and inorganic solids, salts and chemicals added during processing operations are produced as wastes (RMAA, 2010; Steffen and Kirsten, 1989). Various parts of cattle such as muscle, blood, liver, kidney, viscera and hair have been found to contain potentially toxic metals (Kruslin et al., 1999; Jukna et al., 2006). The faeces of livestock (animal manure) consist of undigested food, most of which are: cellulose fibre; undigested protein; excess nitrogen from digested protein; residue from digested fluids; waste mineral matter; worn-out cells from intestinal linings; mucus and bacteria. Other components of undigested food include; foreign matter such as dirt consumed, calcium, magnesium, iron, phosphorous, sodium among others (Ezeoha and Ugwuishiwu, 2011). Abattoir effluent waste water has a complex composition and can be very harmful to the environment. For example, discharge of animal blood into streams would deplete the dissolved oxygen (DO) of the aquatic environment. Improper disposal of paunch manure may exert oxygen demand on the receiving environment or breed large population of decomposers (micro-organisms), some of which may be pathogenic. Also, improper disposal of animal faeces may cause oxygen-depletion in the receiving environment. It could also lead to eutrophication of the receiving system and increase rate of toxins accumulation in biological systems (Nwachukwu et al., 2011).

Mohammed and Musa (2012) reported that the improper disposal of abattoir effluent could lead to transmission of pathogens to human which may cause an outbreak of water borne diseases like diarrhoea, pneumonia, typhoid fever, asthma, wool sorter diseases, respiratory and chest diseases. Studies have shown that *Escherichia coli* infection source was reported to be undercooked beef which has been contaminated in abattoirs with faeces containing the bacterium (Bello and Oyedemi, 2009; Patra et al., 2007). It had also been reported that abattoir activities are responsible for the pollution of surface and underground waters, reduction of air quality as well as quality of health of residents within the surrounding environment (Katarzyna et al., 2009; Odoemelan and Ajunwa, 2008).

The above situations were even more worrisome in the developing countries where research efforts towards monitoring the environment have not been given the desired attention by the stake holders (Adesemoye et al., 2006).

The main purpose of this work therefore, is to study the pollution status of surface water around Yauri abattoir and assess whether the pollution load is sufficient to affect the health of the inhabitants of the areas who depend on this stream as their source of domestic and irrigation water. The results of the study will assist the regulatory bodies monitor more closely the activities at the abattoir as well as create public awareness about the health implications of abattoir activities on the environment and also establish a data bank for future reference.

MATERIALS AND METHODS

The study area

Yauri town in Yauri Local Government Area of Kebbi state, northwestern Nigeria was the study area. It is located southward on the earthen bank of River Niger and falls within latitudes 10°N and 30°N and longitudes 3°W and 6°W of the globe. The area has flat topography with a few elevated areas. It is an extension of the Sokoto plain: dotted with some doom-shaped hills and complemented by a portion of the great River Niger and its numerous tributaries, which gently meanders on the landscape. Yauri abattoir is located some meters from Yauri main market close to Yauri River. Several animals (cows, goats, sheep and cattle) are slaughtered in this abattoir. Normal abattoir operations are carried out every day of the week during morning hours (5 to 11 am) and in the afternoon and evening when the need arise.

Sample collection

Six sampling stations were mapped out along the course of the river in the abattoir area at a distance of 50m from each other. The sampling stations were coded SS_1, SS_2, SS_3, SS_4, SS_5 and SS_6. Six replicate samples were collected from each of these stations and pooled together to obtain a representative sample for that station. Water sample (coded SS_{ctrl}) was collected at a point 60m upstream, and served as a control. Water samples were collected in plastic containers previously cleaned by washing in non-ionic detergent. During sampling, sample bottles were first rinsed with the sampled water three times and then filled to the brim. The samples were labeled and transported to the laboratory, stored in a refrigerator at about 4°C prior to analysis (Akan et al., 2010). A total of forty two samples were collected for the research. The field research is carried out between the months of July and December, 2012.

Sample preparation and analysis

Each sample (100 ml) was transferred into a beaker and 5ml of concentrated HNO_3 was added. The beaker with the content was placed on a hot plate and evaporated down to about 20 ml. The beaker was cooled and another 5 ml of concentrated HNO_3 added. Each beaker was then covered with a watch glass and returned to

Table 1. Mean concentration (mg/L) of potentially toxic metals in the water sample around Yauri Abattoir.

Sampling points	Cd	Co	Cu	Fe	Ni	Pb	Zn
SS_1	22.30±0.03	8.13±2.10	10.21±0.11	50.60±1.30	49.03±2.30	40.51±0.34	62.14±0.04
SS_2	13.10±0.13	3.01±0.70	8.13±2.10	77.02±0.11	18.70±1.00	66.13±0.41	41.07±0.59
SS_3	5.09±0.30	11.68±0.50	19.32±4.40	63.50±0.70	31.61±1.30	38.14±0.03	29.46±1.01
SS_4	8.14±0.21	9.40±0.47	22.31±1.50	48.17±0.50	56.06±0.40	32.10±1.50	31.47±0.09
SS_5	10.07±0.11	7.34±0.09	15.65±2.03	89.11±0.31	30.20±1.60	18.63±1.05	57.72±0.25
SS_6	9.47±0.08	2.03±1.32	11.06±1.30	56.55±2.30	27.31±0.50	56.13±0.01	60.13±0.11
SS_{ctrl}	2.07±1.04	0.63±0.02	5.53±2.30	36.20±2.60	0.59±1.33	22.01±2.01	20.52±0.10
Range	5.09- 22.30	2.03-11.68	10.21-89.11	48.17-89.11	18.70-56.06	18.63-66.13	29.46-62.14
HQ	631.00	641.00	10.85	5.94	49.29	3.88	4.35
EPA*	0.25	23.00	9.00	300.00	52.00	2.5.00	120.00
EU	0.005	N/A	2.00	0.20	0.02	0.01	N/A
WHO	0.003	N/A	2.00	N/A	0.02	0.01	3.00

N/A = Not Available, * = ug/L.

the hot plate for more heating with the addition of few drops of HNO_3 until the solution appeared light coloured and cleared. The walls of the beaker and the watch glass were washed down with distilled water and the sample filtered to remove insoluble materials that could clog the atomizer. The volumes of the samples were made up to the mark (100 ml) with distilled water (Radojevic and Bashkin, 1999). A blank sample was similarly treated so as to give room for blank correction. This was done by transferring 100ml of distilled water into a beaker and digested as described above. Calibration standards were prepared from stock solutions by dilution and were matrix matched the acid concentration of the digested samples. The digested samples were then analyzed for potentially toxic metals using atomic absorption spectrophotometer alpha star model 4 (Chem Tech Analytical) at the Centre for Energy Research and Development of the Obafemi Awolowo University, Ile–Ife, Nigeria. The instrument was operated according to the instrument handbook and data were acquired with Hewlett Packard (HP) Pavilion 3134 software.

The method used for the determination of physicochemical parameters was as described by AOAC (2005) and reported elsewhere (Anon, 1992; Lovell and Colorado, 1983; Ademorati, 1996 Emmanuel and Solomon, 2012).

RESULTS AND DISCUSSION

Potentially toxic metals concentration

Table 1 is presented the mean concentrations (mg/L) of potentially toxic metals in surface water from Yauri. The results show differences in metal concentrations at various sampling stations and their controls. Iron was the most abundant metal recorded. The higher level of Fe recorded within the study area could be related to run-off from rusted metallic roofing sheets on the houses in the area, scrap metal dump sites and the abattoir refuse dump sites. All the metals with the exception of Cd, Ni and Pb were below the international maximum permissible limit (WHO, 2006; EU, 1998).

The sources of cadmium in the urban areas are much less well defined than those of lead, but metal plating and tire enforced with metals were considered the likely common anthropogenic sources of Cd in the street dust through burning of tires and bad roads. Cadmium high mean concentration levels at all the sampling points could be attributed to the above reason and in addition to rural/urban effluents along the river course and atmospheric precipitation. Cadmium is extremely toxic that it could cause adverse health effects to end user when water with high percentage is consumed and it is also toxic to fish and other aquatic organisms.

Lead and Nickel concentrations within the study area is pointed to the fact that naturally, Pb and Ni are distributed in surface waters due to weathering of minerals and atmospheric deposition. Also, Lead and Nickel recorded high values beside the abattoir activities could be related to technical uses, most of which are: electric storage batteries, leachate from sludge containing nickel-cadmium batteries, nickel plate items and emissions from burning of fossil fuels and gasoline which contain high levels of tetraethyl lead (TEL), which is still in use despite, its ban in 2004. Generally, the concentration of metals in water in the study area is higher than the control. It has been reported that potentially toxic metals, reaching excessive levels, can exert serious impact on humans, animals and plants because they are not biodegradable as they are retained indefinitely in the ecological systems and in the food chain (Omprakash et al., 2011).

Physicochemical evaluation

The physicochemical parameters derived from surface water in Yauri around the abattoir are listed in Table 2. It could be seen from the table that the temperature range is from 30.20 to 30.80°C which is lower than 32 to 34°C reported by Osibanjo and Adie (2007). Temperature

Table 2. Mean results of the physicochemical parameters of the abattoir's surface water.

Parameter	SS_1	SS_2	SS_3	SS_4	SS_5	SS_6	SS_{CRTL}	Range
T (°C)	28.40±0.03	31.30±0.10	30.70±2.10	31.80±1.00	30.50±0.09	30.40±1.15	30.40 ±0.11	30.2-30.8
pH	5.30±0.09	7.55±2.11	6.50±1.70	6.50±0.73	6.56±0.91	6.51±0.27	6.70 ±1.42	6.50-6.70
TDS (mg/L)	630.0±3.17	710.0±3.10	2700.0±1.08	1320.0±2.10	260.0±1.00	540.7±2.40	110.0±5.10	250-700
TSS (mg/L)	330.6±1.01	680.3±1.70	1070.0±0.97	720.14±2.14	400.23±0.9	190.0±1.01	12.0±0.09	190-710
DO (mg/L)	3.10±0.00	2.60±0.10	6.00±0.07	8.00±0.00	4.00±0.01	5.00±2.01	5.90±0.02	2.00-9.00
Sulphate (mg/L)	35.064±0.25	41.60±0.89	170.00±0.90	120.00±1.00	95.11±2.05	60.00±5.01	12.00±0.03	38.46-170
Phosphate (mg/L)	8.00±1.00	7.30±0.03	9.10±3.01	16.00±1.09	8.00±0.90	4.70±0.10	2.10±0.03	4.70-16.0
Nitrate (mg/L)	9.40±0.25	31.09±3.20	68.00±1.08	64.06±0.04	9.30±0.10	66.00±4.02	6.00±0.00	9.30-68.0
BOD (mg/L)	350.50±5.01	516.00±0.05	861.70±4.07	812.60±0.90	344.00±0.30	23.00±0.04	12.00±0.08	19.00-861
COD (mg/L)	540.03±1.06	1452.0±5.01	1508.0±9.03	928.0±0.98	444.0±3.04	548.0±1.90	156.0±0.06	444-1508

influences the amount of dissolved oxygen in water which in turn influences the survival of aquatic organisms. The pH ranged from 6.50 to 6.70 with a mean value of 6.60 and falls within WHO standards and compares well with 4.9 to 7.2 reported by Masse and Masse (2002). Total Suspended Solids (TSS) and Total Dissolved Solids (TDS) values ranged from 190.00-710.14 and 250.00-2700.00 mg/L respectively. Their mean values are 565.22 and 1,026.78 mg/L TSS and TDS respectively which, is above WHO maximum permissible limit for TSS (20 mg/L) and TDS (200 mg/L) and also higher than the control. Total suspended solids relatively measures the physical or visual observable dirtiness of a water resource while TDS is an indicator of the degree of dissolved substances, such as metal ions in the water (Efe et al., 2005). Dissolved oxygen (DO) has a range of 2.0 to 9.0mg/L with a mean value of 50 mg/L. This value is higher than international permissible limit of 4 mg/L and also, higher than the control. Low DO may result in anaerobic conditions that cause bad odour. Biochemical Oxygen Demand (BOD) and Chemical Oxygen Demand (COD) ranges between 19.0-861.7 and 444-1508 mg/L with mean values of 484.63 and 903.3 mg/L respectively. The mean value for BOD is higher than the control and allowable limit of 20 mg/L (WHO, 2006). COD has a mean value lower than the permissible limit of 1000 mg/L. Though, the mean value of COD is lower, some points like SS_2 and SS_3 have values of 1,456 and 1,508 mg/L respectively which are higher than the international standards. Both BOD and COD are indices of organic pollution. BOD is not a specific pollutant indicator, but rather a measure of the amount of oxygen required by bacteria and other microorganisms engaged in stabilizing decomposable organic matter over a specified period of time. A high oxygen demand indicates the potential for developing Dissolved Oxygen sag as the microbiota oxidizes the organic matter in the water. Since nearly all organic compounds are oxidized in the COD test, COD results are always higher than BOD results. This was confirmed in this study with some samples (SS_2 and SS_3) exceeding the value of 1000 mg/L set by WHO.

Nitrate concentration ranges from 9.4 to 68 mg/L with a mean value of 41.45 mg/L. Even though the mean concentration value is low, some points analyzed have values higher than the set standards. It is reported that nitrate concentration above the permissible value by 45 mg/L is dangerous to pregnant women and poses a serious health threat to infants less than three to six months of age because of its ability to cause methaemoglobinaemia (Gelperim et al., 1975). Nitrates have a high potential to migrate into ground water since they are very soluble and do not bind to soil (Punmia and Jain, 1998). Phosphates were at relatively high concentration. All the water samples were above 5mg/L maximum permissible limit except for SS_6 (4.7mg/L). Phosphate enter water ways from human, animal waste and other sources like phosphorus rich bedrock, industrial effluents, fertilizer run-off, laundry and cleaning. Phosphates in water increase the tendency of troublesome algae to grow in the water (Esry et al., 1991). This causes eutrophication or over fertilization as it chokes up the water ways and uses up large amounts of oxygen. Sulphate concentration ranges from 40 to 170 mg/L with a mean value of 86.91 mg/L. This is lower than the maximum permissible limit of 250 mg/L set by WHO but higher than the control value of 12 mg/L. This implies that the activities in the abattoir are contributing to the pollution load of the stream and long term effect may subsequently lead to contamination of the surrounding water body.

Health risk assessment

Health risk assessment is normally based on a quantification of risk level in relation to two types of adverse effects: chronic (non-carcinogenic) and carcinogenic. Chronic risk level estimated was expressed as maximum hazard quotient (HQ_{max}) calculated for a group of evaluated elements and as hazard index (HI) calculated as a sum of HQ of all evaluated elements in every sample ($HI=\Sigma HQ_i$). Characterisation of the chronic risk level consists of threshold effects (tolerance chemical

Table 3. Correlation Matrix for pairs of the analyzed potentially toxic metals in water.

Metals	Cd	Co	Cu	Fe	Ni	Pb	Zn
Cd	1.000						
Co	0.334	1.000					
Cu	0.240	0.113	1.000				
Fe	0.249	-0.042	0.787*	1.000			
Ni	0.552	0.169	0.712	0.797*	1.000		
Pb	0.025	0.073	0.039	0.161	0.391	1.000	
Zn	0.365	0.060	-0.194	0.162	0.011	0.318	1.000

* Correlation is significant at the 0.05 level (2-tailed).

level) and is based on the presumption and manifestation of adverse chronic effects until the threshold, that is, the lifetime daily exposure level tolerated by human beings the so-called reference dose (RfD), is exceeded. The characterisation of carcinogenic risk level consists of a concept of non-threshold effects – that is, no dose is safe and risk-free and each level of exposure can generate a carcinogenic response (USEPA, 1989).

In the present study, health risk from increased concentrations of HM in the surface water was evaluated in relation to its chronic as well as carcinogenic effects, based on the calculation of average daily dose estimates and defined toxicity values for toxic HM (USEPA, 1999) according to the following relationships. The chronic risk level was computed as health risk assessment using CDI and HQ indices. The CDI through water ingestion was calculated using the USEPA (1992) equation below:

$$CDI = C \times DI/BW$$

Where C, DI and BW represent the concentration of HM in water (microgrammes per litre), average daily intake rate (2 L/ day) and body weight (72 kg), respectively (USEPA 2005).

Conversely, the chronic risk level was calculated (HQ) for non-carcinogenic risk using the following equation by USEPA (1999):

$$HQ = CDI/RfD$$

Where according to USEPA, the oral toxicity RfD values are 0.0005 mg/kg-day for Cd, 0.0003 mg/kg-day for Co, 0.037 mg/kg-day for Cu, 0.3 mg/kg-day for Fe, 0.02 mg/kg-day for Ni, 0.0036 mg/kg-day for Pb and 0.3 mg/kg-day for Zn, respectively.

The scale of chronic risk level (HQ) based on average daily intake (CDI) and reference dose (milligrammes per kilogramme-day) is classified based on the ratio of CDI/RfD indicating≤1 (no risk) if>1≤5 (low risk), if>5≤10 (medium risk) and if>10 (high risk).

Correlation analysis

One-way analysis of variance with parametric Pearson's correlation between mean potentially toxic metals concentration in the water samples standard statistical methods (Table 3) showed that all the metals were positively correlated except for Fe and Co and Zn and Cu which were negatively correlated. Pb, Cd, and Ni were significantly correlated. The positive and significant correlations between metals in the surface water samples suggest common source.

Conclusions

The results of this study revealed that the physicochemical parameters of the surface water around Yauri abattoir exceeded international recommended safe limits. The mean concentrations of Pb, Ni and Cd were also higher than the regulatory permissible limits. The positive correlations between the pairs of metals in the surface water suggest common anthropogenic source. Generally, the values of the physicochemical parameters and potentially toxic metals were higher in the surface water around the abattoir than the control samples. This implies that the activities at the Yauri abattoir were contributing to the pollution load of the surface water in the area and this has potential for full-blown environmental problems in the near future if not controlled. It is therefore, recommended that the activities of the abattoir should be monitored closely by relevant agencies and constant monitoring of the river water quality is needed to record any alteration in the quality and mitigate outbreak of health disorders and the detrimental impacts on the aquatic ecosystem and through bio-magnifications may enter the food chain thereby affecting the human beings as well.

Conflict of Interest

The authors have not declared any conflict of interest.

REFERENCES

Ademorati CM (1996) . Standard methods for water and effluents

analysis. Foludex Press Ltd, Ibadan. pp. 20-49.
Adesemoye AO, Opere BO, Makinde SC (2006). Microbial Content of abattoir waste water and its contaminated soil in Lagos, Nigeria. Afr. J. Biotechnol. 5(20):1963-1968.
Akan JC, Abdulrahman FI, Yusuf E (2010). Physical and chemical parameters in Abattoir waste water sample in Maiduguri metropolis, Nigeria. The pacific J. Sci. Tech. 11(1): 640-647.
Alorge DO (1992). Abattoir Design, Management and Effluent Disposal in Nigeria, University of Ibadan press.
Anon R (1992). Standard methods of Water and Wastewater Examination. 18th edition American Public Health Association Washington, D. C. 2:172.
AOAC (2005). Official Method of Analysis Association of Analytical Chemist. Washington, DC, 15th ed. 11–14.
Bello YO, Oyedemi, DT (2009). The impact of abattoir activities and management in residential neighbourhoods: A case study of Ogbomoso, Nigeria. J. Soc. Sci. 19(2):121-127.
Efe SI, Ogban FE, Horsfall M, Akporhornor EE (2005). Variation of physicochemical characteristics in water resources quality in Western Niger delta region, Nigeria. J. Appl. Sci. Environ. Man. 9:191-193.
Emmanuel OO, Solomon A (2012). Quality of sachet water and bottled water in Bolgatanga Municipality of Ghana. Res. J. Appl. Sci. Eng. Tech. 4(9):1094-1098.
Esry SA, Potash JB, Shiff C (1991). Effects of improved water supply and sanitation on ascariosis, diarrhea, dracunculiasis, hookworm infection, schistosomiasis and tachorna. Bulletin of WHO (5):610-614.
EU (1998). European Union Drinking Water Standards http://www.lenntech.com/EU's-drinking-water-standards.htm.
Ezeoha SL, Ugwuishiwu BO (2011). Status of abattoir wastes research in Nigeria. Nig. J. Technol. 30(2).
Gelperim A, Moses UK Bridge C (1975). Relationship of high nitrate community water supply to infants and fetal mortality. Illinois's Med. J. 147:155-156.
Jukna C, Jukna V, Suigzdaite J (2006). Determination of potentially toxic metalss in Viscera and Muscles of cattle. Bulgarian J. Vet. Med. 9(1):35-41.
Katarzyna RA, Monkiewicz J, Andrzej G (2009). Lead, Cadmium, Arsenic, Copper and Zinc contents in hair of cattle living in the area contaminated by a copper smelter in 2006-2008. Bull. Vet. Inst. Pulawy. 53:703-706.
Kruslin E, Hodel CM, Schurgast H (1999). Progress in diagnosis of chronic toxic metal poisoning by hair analysis. Toxicol. Lett. 88:84.
Lovell J, Colorado W (1983). Hach Water Analysis Hand book: 181-278.
Masse DI, Masse L (2002). Characterisation of effluents from six hog slaughter houses in Eastern Canada and evaluation of their impact influent treatment systems. Canada J. Agric. Eng. 42:139-146.
Mohammed S, Musa JJ (2012). Impact of Abattoir Effluent on River Land Use, Bida, Nigeria. J. Chem. Bio. Phys. Sci. 2(1):132-136.
Nwachukwu MI, Akinde SB, Udujih OS, Nwachukwu IO (2011). Effect of abattoir wastes on the population of proteolytic and lipolytic bacteria in a Recipient Water Body (Otamiri River). Global Res. J. Sci.1(1):40 – 422.
Odoemelan SA, Ajunwa O (2008). Potentially toxic metals status and physicochemical properties of agricultural Soil amended by short term application of animal manure. J. Chem. Soc. Nig. 30:60-63.
Olanike KA (2002). Unhygienic operation of a city abattoir in South Western Nigeria: Environmental implication *AJEAM/RAGEE.* 4(1): 23-28.
OmPrakash M, Ashish G, Mahipat S, Rajay P (2011). Determination of Toxic Trace Metals Pb, Cd,Ni, and Zn in Soil by Polarographic Method. Int. J. Chem. Tech. Res. 3(2):599-604.
Osibanjo O Adie GU (2007). Impact of effluent from Bodija Abattoir on the physicochemical parameters of Oshunkaye stream in Ibadan. Afr. J. Biotech. 6(15):1806-1811.
Patra RC, Swarup D, Naresh R, Kumar P (2007). Tail hair as an indicator of environmental exposure of Cows to lead and cadmium in different industrial areas. Eco. Toxicol. Environ. 66:127-131.
Punmia BC Jain AK (1998). Wastewater Engineering. Laxmi publications, New Delhi.
Radojevic M Bashkin VN (1999). Practical Environmental Analysis. The Royal Society of Chemistry: Cambridge, UK. 466.
Red Meat Abattoir Association (RMAA). (2010). Waste Management-Red Meat Abattoir. Retrieved from http://www.docstoc.com/docs/103302144/Waste-Management-%EE%9F%A6-Red-Meat-Abattoirs.
Steffen, Roberts, Kirsten Inc. (1989). Water and waste-water management in the red meat industry. (P. 36). WRC Report No. 145 TT41/89. WRC, Pretoria.
United States Environmental Protection Agency (USEPA) (1989). Risk assessment guidance for superfund (RAGS): volume I- Human health evaluation manual (HHEM) part A: baseline risk assessment, Interim Final (EPA/540/1-89/002). Office of Emergency and Remedial Response, Washington, DC.
United States Environmental Protection Agency (USEPA) (1992). Guidelines for Exposure Assessment, EPA/600/Z-92/001. Risk Assessment Forum, Washington, DC.
United States Environmental Protection Agency (USEPA) (1999). Guidance for performing Aggregate Exposure and Risk Assessment office of Pesticide Programs, Washington, DC.
United States Environmental Protection Agency (USEPA) (2005). Guidelines for carcinogen risk assessment. Risk Assessment Forum, Washington, DC (EPA/630/P-03/001F).
World Health Organization (WHO). (2006). Drinking Water Standards, .http://www.lenntech.com/WHO's-drinking-water-standards06.htm.

academicJournals

Vol. 9(3), pp. 39-49, March, 2015
DOI: 10.5897/AJPAC2015.0607
Article Number: 2A845A651545
ISSN 1996 - 0840

http://www.academicjournals.org/AJPAC

African Journal of Pure and Applied Chemistry

Full Length Research Paper

Corrosion and corrosion inhibition of cast Iron in hydrochloric acid (HCl) solution by cantaloupe (*Cucumis melo*) as green inhibitor

Khadijah M. Emran[1]*, Arwa O. Al-Ahmadi[2], Bayan A. Torjoman[2], Najla M. Ahmed[2] and Sara N. Sheekh[2]

[1]Chemistry Department, Faculty of Science, Taibah University, Saudi Arabia.
[2]Chemistry Department (Applied Chemistry), Faculty of Science, Taibah University, Saudi Arabia.

Received 10 January, 2015; Accepted 27 January, 2015

The effect of cantaloupe juice and seed extracts on corrosion of cast iron in 1.0 M hydrochloric acid (HCl) solution using hydrogen evolution measurements (HEM) and mass loss measurements (MLM) were investigated. Cantaloupe extracts inhibited the corrosion of cast iron in 1.0 M HCl solution. The inhibition efficiency increased with concentration of the extracts. The adsorption of the inhibitor molecules on cast iron surface was in accordance to Langmuir adsorption isotherms. In absence of inhibitors, the corrosion rate of cast iron increases with HCl concentration. The fractional reaction order observed in HCl solution indicates the formation of intermediates through the dissolution process or multiple steps mechanism of cast iron dissolution in HCl solution.

Key words: Cantaloupe (*Cucumis melo*), corrosion, cast iron, HCl concentrations, adsorption isotherm.

INTRODUCTION

The use of inhibitors is one of the best options of protecting metals against corrosion, especially green or eco-friendly inhibitors. Now, this field has been promising and effective, and it can be extracted by simple and inexpensive procedures. Comparisons have been made through the years between the toxic inorganic inhibitors such as; chromates, pomegranate, and cyanide, or synthetic organic compounds and the natural inhibitors, it observed that the natural inhibitors could potentially serve as an effective substitute for the corrosion inhibitors without constituting risk for human health or the environment in which people live in (Shanableh, 2011). Many of these natural inhibitor substances can be extracted from different parts of plants: seed, fruit and leaves. Anyway, the plant extracts are considered as a rich source of environmentally acceptable corrosion inhibitors. For being that it can be extracted by simple procedures, which can keep the environment healthier with low cost and can be applied in various aggressive environments that make it a major importance in research

*Corresponding author. E-mail: kabdalsamad@taibahu.edu.sa

Figure 1. Cantaloupe *(Cucumis Melo)*.

and studies.

Acidic solutions are widely used in various industries for pickling ferrous alloys and steel. They are also used in oil and gas production to stimulate and increase the oil and gas flow to disqualify encrustations in production wells. Among various acids, the hydrochloric acid is mostly used for this purpose. Due to the extremely aggressive nature of acidic media, localized pitting corrosion starts to occur on the metal surface, over time, produces damage and destruction for products (Gadow and Fouda, 2014). In contrast, the particles of inhibitor are commonly used to reduce acid attack on the substrate metal by blocking active sites against deterioration.

Various natural plants are now used in many industries to protect steel in hydrochloric acid (HCl) solution, example, *Garcinia Mangostana* extract (Kumar et al., 2010), *Black pepper* extract (Damani et al., 2010), *Fenugreek* seed (Bouyanzer et al., 2010), Fennel *(Foeniculum Vulgare)* (Lahhit et al., 2011) and *Grap Pomace* (Rocha et al., 2012).

Cantaloupe (*Cucumis melo*) figure 1, a kind of muskmelon fruit belonging to the family Cucurbitaceae table 1, which is native to India and Africa. The unique aroma of cantaloupe is composed of many volatile compounds, biosynthetically derived from; fatty acids, carotenoids, amino acid and terpens (Nattaporn and Pranee, 2011; Milind and Kulwant, 2011). This article report the effect of cantaloupe juice and seed extracts as corrosion inhibitors of cast iron in 1.0 M HCl solution, using hydrogen evolution measurements (HEM) and mass loss measurements (MLM). In our knowledge, this is the first time that cantaloupe juice and seed extracts have been used as inhibitor of cast iron in HCl solution. Reinforced by the discussion of other study, common adsorption isotherms determine a process and nature of inhibitors adsorption, aim to choose the best adsorption isotherm curves that fit with experimental data (Figure 1 and Table 1).

Table 1. Scientific classification of cantaloupe *(Cucumis Melo)*.

Kingdom	**Plantae**
Subkingdom	Tracheobionta
Super Division	Spermatophyta
Class	Mangoliophyta
Family	Cucurbitaceae
Genus	Cucumis L.
Species	*C. Melo var. Cantalupensis*

EXPERIMENTAL

Materials and solutions

Test was performed on cast iron specimen with weight percentage compositions in Table 2. The cast iron specimen was manufactured as cylindrical and purchased from ATTAIH Company, KSA. Before all measurements, the specimen was polished with a series of abrasive paper finding a coarse to remove roughness and rust. After that, the sample was washed by double-distillated water and acetone, and finally dried for weighted. The HCl solution was studied for Analar grade reagents. The solution was freshly prepared by double-distilled water in range (0.5 to 2.0 M) concentration by analytical dilution of stock solution (37%).

Cantaloupe extracts preparations

The juice extract of cantaloupe was obtained by putting fresh pulp for five cantaloupes in the blender, then filtered to get homogenous solution. While, the stock solution of seed extract was prepared by boiled weight grams of dried seed in 600 ml from double-distilled water for 90 min. The extract filtered and completed to 500 ml by double-distilled water. Both extracts kept freshly in refrigerator.

Gravimetric and volumetric measurements

The measurements were carried out by tow method; hydrogen evolution (HEM), and mass loss (MLM). Evolved H_2 was collected in a calibrated tube by downward displacement of water over time. The temperature was adjusted at room temperature 27°C by thermostat. The rates of HEM (R, ml/cm^2.min) and MLM (R_w, g/cm^2.min) were calculated as related in Equations (1) and (2), respectively (Mathur and Vasudaven, 1982; El-Etre, 2003):

$$R = \frac{\Delta V/A}{t} \quad (1)$$

$$R_w = \frac{W_1 - W_2}{A\ t_f} \quad (2)$$

Where ΔV is the displacement of evolved gas, t is the time for evolved gas in minute, W_1 and W_2 are the mass of cast iron specimen before and after immersion in tested solution, respectively, t_f is the final time of experiment and A is the surface area of cylindrical specimen in cm^2.

The specimen was immersed in 1.0 M HCl solution in presence inhibitors at 27°C. The inhibition efficiency (*%IE*) and degree of

Table 2. Chemical compositions of cast iron specimen with weight percentage (%W).

%C	%Si	%Mn	%P	%S	Remain
3.45 - 3.65	2.40 - 2.70	0.60 – 0.70	0.17 – 0.26	0.04 – 0.06	Fe

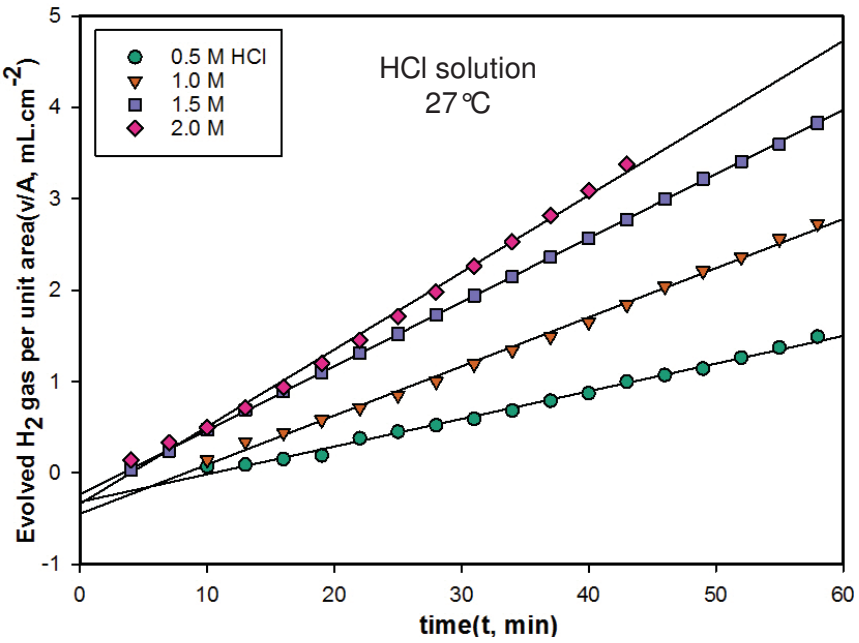

Figure 2. Volume of evolved H_2 per unit area versus exposure time for cast iron corrosion in various concentrations of HCl solutions at 27°C.

surface coverage (θ) were calculated from both HEM and MLM by Equations (3), (4), (5) and (6) respectively (Oguzie, 2007).

$$\%IE_{HEM} = \frac{R - R'}{R} \times 100 \quad (3)$$

$$\theta = \frac{R - R'}{R} \quad (4)$$

$$\%IE_{MLM} = \frac{R_\circ - R'_\circ}{R_\circ} \times 100 \quad (5)$$

$$\theta = \frac{R_\circ - R'_\circ}{R_\circ} \quad (6)$$

Where R and $R_\circ$ are the HEM and MLM in the absence inhibitor, respectively. While R' and $R'_\circ$ are HEM and MLM in presence inhibitor, respectively.

The corrosion rate for MLM (C.R, mmy) of the cast iron was also calculated by using the following (Equation 7) (Quraishi et al., 2009):

$$C.R.(mmy) = \frac{87.6W}{AtD} \quad (7)$$

Where W is the weight loss of the metal (mg), A is the surface area of the metal specimen (cm^2), t is the exposure time (h) and D is the density of the metal (g/cm^3).

RESULTS AND DISCUSSION

Behavior of cast iron (CI) corrosion in various concentrations of HCl solutions at 27°C

The data plotted for volume of evolved H_2 per unit area against time in minutes for 0.5 to 2.0 M of HCl concentrations at 27°C, is presented in Figure 2. The slopes of such lines were estimated in Table 3, taken as rates of cast iron corrosion reacted with HCl solution as corrosive environment using HEM. It is clear after inspection through duration experiment; the volume of evolved H_2 gas per unit area (V/A) increase upon increasing concentration.

The rates of corrosion of cast iron in various

Table 3. The corrosion rates of HEM & MLM for corrosion of cast iron in various concentrations of HCl solutions at 27°C.

HCl Concentration(M)	0.5	1.0	1.5	2.0
R_{HEM} (mL.cm^{-2}.min)	0.030	0.054	0.070	0.084
R_{MLM} (g.cm^{-2}.min)	6.90x10^{-5}	1.06x10^{-4}	1.28x10^{-4}	1.71 x10^{-4}
C.R. (mmy)	49.59	73.53	88.77	119.34

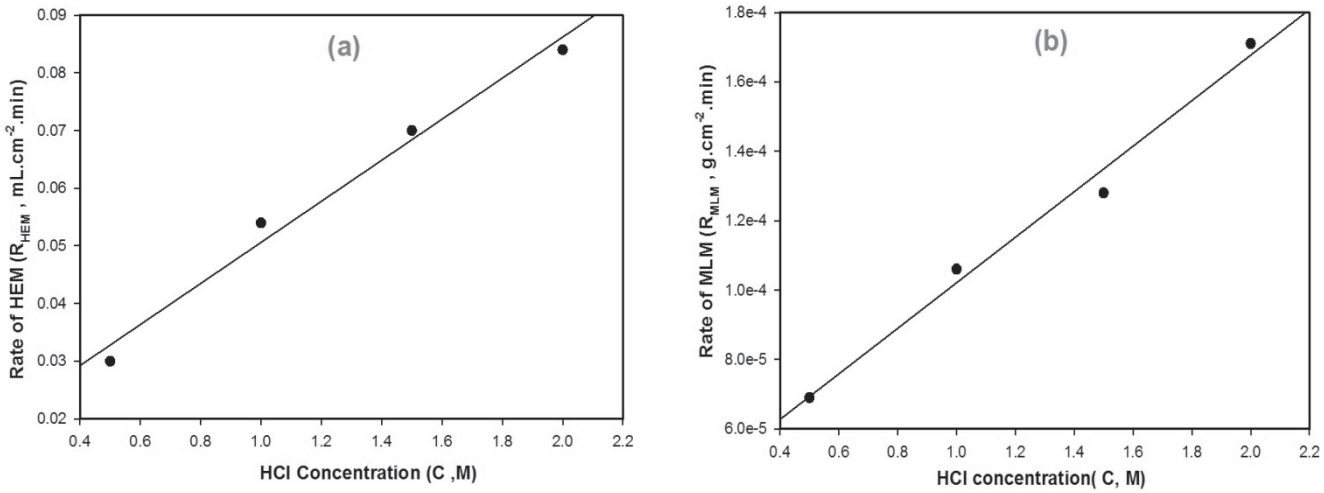

Figure 3. Rate (a) HEM (b) MLM of cast iron corrosion against various concentrations of HCl solutions at 27°C.

concentrations of HCl solutions resulted from HEM, constructed that by MLM after weight specimen; which were characterized by rapid effervescence, this influence is shown in Figure 3. The C.R. (mmy) of cast iron increase with increasing acid concentration, this indicates that cast iron corrosion in HCl is concentration dependent. It can also be observed from the Table 3 and Figure 3 a very good agreement between values of corrosion rates obtained from the three methods.

This result was expected, because with increased acidic concentration; both acidity and Cl^- anions concentration are increased too. This observation agrees with the fact that the rate of chemical reaction, diffusion, and ionization activates with increased concentration (Al-Tturkustani et al., 2010).

The straight line shown in Figure 2 when a metal reacted with aggressive solution caused rapid reaction between acid, and air indicates a soluble passive layer (oxide film) formed on the surface of cast iron. As well, the presence of "induction period" at the beginning of the interaction (this obvious at 0.5 M) means dissolution of the formed oxide layer. It leads to none protection occurring on the surface and prevented solution from coming to the surface. This layer starts to fade rapidly with increase concentration of aggressive solution especially up to 2.0 M HCl solution. This concentration gives very good identity in linearity, the attack on oxide film by Cl^- anions was instantaneous, forming local thinning passive layer on metal surface, over time create pitting localized corrosion (Al-Tturkustani et al., 2010). Generally, the corrosion of iron in HCl solution revealed that it (Popova et al., 2005) takes place with hydrogen depolarization. The spontaneous dissolution of iron can be described by anodic dissolution reaction (Equation 8), accompanied by the corresponding cathodic reaction (Equation 9):

$$Fe \rightarrow Fe^{2+} + 2e \quad (8)$$

$$2H^+ + 2e \rightarrow H_2 \uparrow \quad (9)$$

The corrosion of metals in acidic solution is cathodically controlled by the hydrogen evolution reaction which occurs in two steps (Equations 10 and 11) according to (Mathur and Vasudaven, 1982):

$$H^+ + e \rightarrow H_{ads} \quad (10)$$

$$H_{ads} + H_{ads} \xrightarrow{r.d.s} H_2 \uparrow \quad (11)$$

The rate determining step for the hydrogen evolution

Table 4. Kinetics parameters of the Mathur and Vasudevan model and conventional model.

Methods	Mathur and Vasudevan model			Conventional model		
	ln k	B	R2	lnk	n	R^2
HEM	-3.52	0.57	0.99	-2.88	0.60	0.99
MLM	-9.82	0.58	0.98	-9.15	0.63	0.98

reaction is the recombination of adsorbed hydrogen evolution reaction which the recombination of adsorbed hydrogen atoms form hydrogen molecules (Equation 11). Corrosion rate data as a function of acid concentration can be used to show the rate dependence of hydrochloric acid concentration by Mathur and Vasudevan model (Equation 12) and based on the kinetic equation (Equation 13) (Mathur and Vasudaven, 1982):

$$\ln R = \ln k + BC \quad (12)$$

$$\ln R = \ln k + n \ln C \quad (13)$$

Where *R* is the rate of metal dissolution, *k* is corrosion rate constant, B and *n* is the reaction order and C molar concentration of HCl solution.

The values of *k, B* and *n* obtained using HEM and MLM data and listed in Table 4. The fractional order observed in HCl solution may indicate the formation of intermediates through the dissolution process (Zaafarany, 2012), or multiple steps mechanism of cast iron dissolution in HCl solution.

Inhibition action of cantaloupe extracts as green inhibitor in cast iron corrosion

The corrosion rates for cast iron in 1.0 M HCl in absence and presence of cantaloupe extracts were determined by using HEM and MLM. Figure 4 shows the variations of evolved H_2 with time during the corrosion of cast iron in 1.0M HCl for various concentrations of cantaloupe extracts (a) juice and (b) seed at 27°C. The corresponding values of corrosion rates were given in Table 5 from slope of each line.

In comparison, blank solution (absence inhibitors) with added various concentrations of inhibitors (%v/v) of juice and seeds extracts; were noted with straight lines with much lower decreased rather than blank solution. The decline become even more with increased concentration of juice or seeds extracts. This indicates to oppositely occur when studied behavior of cast iron corrosion in HCl solution and the passive layer (adsorption film) formed presence inhibitor become insoluble, that inhibitors were first adsorbed onto the surface after impede corrosion process.

The adsorption of an organic adsorbate between metal/solution interface can be represented as a substitutional adsorption process between the organic molecules in the aqueous solution $Org_{(soln)}$ and the water molecules on the metallic surface $H_2O_{(ads)}$ (Equation 14) (Bockris and Swinkels, 1964).

$$Org_{(soln)} + x\, H_2O_{(ads)} \leftrightarrow Org_{(ads)} + x\, H_2O_{(soln)} \quad (14)$$

where $Org_{(ads)}$ are the organic molecules adsorbed on the metallic surface, $H_2O_{(sol)}$ is the water molecules in the aqueous solution and x is the size ratio representing the number of water molecules replaced by one molecule of organic adsorbate. According to (Bockris and Drazic, 1962) the inhibition mechanism could be explained by the $Fe(inh)_{ads}$ reaction as intermediates:

$$Fe + Inh \Leftrightarrow Fe(Inh)_{ads} \Leftrightarrow Fe^{n+} + n\, e + Inh \quad (15)$$

With further clarification, the $Fe(Inh)_{ads}$ did not have enough covered metal surface at low concentration of inhibitor, maybe because the added low concentration of inhibitors, or the rate adsorption is slow. So, the metal dissolution takes place on sites more than the formed $Fe(Inh)_{ads}$. Otherwise, at high concentration of inhibitor on the cast iron surface forms compact and coherent inhibitor over layer, then reducing chemical attack for metal (Branzoi et al., 2000; Singh and Quraishi, 2012).

The inhibitor efficiency of cantaloupe juice and seed extracts may be due to presence of many organic substance that acts as a good corrosion inhibitors, branched-chain and aromatic amino acid (Gonda et al., 2010; Nattaporn and Pranee, 2011; Milind and Kulwant, 2011). These compounds usually contain polar functions with heteroatoms such as nitrogen, oxygen, sulphur and phosphorus, and have triple or double bonds or aromatic rings. These groups are more a donor of electron and it offers itself the possibility to be a center of adsorption. The adsorption of these organic compounds by deferent centers of adsorption on the electrode surface makes a barrier for mass and charge transfers. This situation leads to a reduction in the double layer and a protection of the metal surface from the attack of the aggressive anions of the aggressive solution (Barouni et al., 2008; Emran et al., 2014).

The plot rates of corrosion HEM and MLM versus concentrations of juice or seeds extracts by (%v/v) at

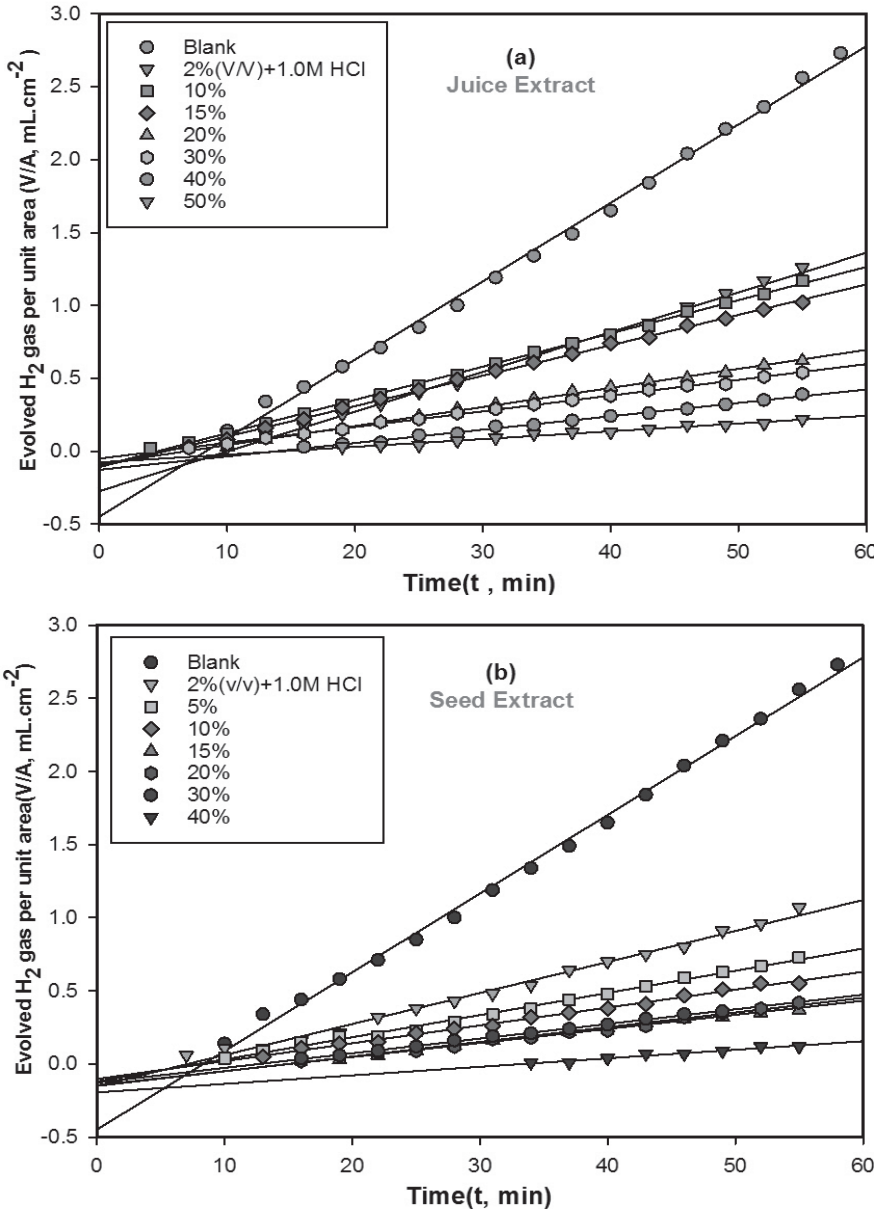

Figure 4. Variations of evolved H_2 for (a) juice (b)seed extracts of cantaloupe in 1.0 M HCl solution at 27°C.

27°C were presented in Figure 5. It is obvious that the added extracts into 1.0 M HCl solution caused noticeable reduction in amount rates obtained on cast iron surface. Seeds extract of cantaloupe has a great decrease in rate of HEM followed by MLM at different concentrations than juice extract. This is precisely what was interpreted in Table 5. 2 ml (%v/v) of juice and seeds extracts, significantly reduced the mass loss of cast iron with a factor 2 and 2.6 times respectively, and arched to 5.87 and 8.71 times at 40 (%v/v) compared with blank respectively. The values of inhibition efficiency of % IE_{HEM}, $\%IE_{MLM}$ degree of surface coverage (θ_{HEM}) and θ_{MLM} were listed in Table 5. The surface coverage and inhibition efficiency values increase with increasing extract concentration (Figure 6). The maximum inhibition efficiency %IE value of 91.11 and 91.16% for juice extract at 50%(v/v), whilst in seeds extract were 91.30% and 88.5% at 40%(v/v) by using MLM and HEM at 27°C, respectively. This is due to the blocking active sites on metal surface and decreasing the effective area of corrosion attack by adsorption of effect compounds present in cantaloupe, like; Vitamin, Phenolic compounds, Terpenoids etc. (Nattaporn and Pranee, 2011; Milind and Kulwant, 2011).

Table 5. Effect of inhibitors on the corrosion of cast iron in 1M HCl solution by using HEM and MLM at 27°C.

Inhibitor concentration %(v/v)		HEM			MLM		
		R_{HEM} (ml.cm^{-2}.min)	$\%IE_{HEM}$	θ_{HEM}	R_{MLM} (g.cm^{-2}.min)	$\%IE_{MLM}$	θ_{MLM}
Blank (1.0 M HCl)		0.054	-	-	1.06x10^{-4}	-	-
Juice extract	2%	0.027	50	0.50	5.30 x10^{-5}	50	0.50
	10%	0.023	57.41	0.57	4.85 x10^{-5}	54.25	0.54
	15%	0.021	61.11	0.61	4.04 x10^{-5}	61.89	0.62
	20%	0.013	75.93	0.76	2.59 x10^{-5}	76.04	0.76
	30%	0.011	79.63	0.80	1.98 x10^{-5}	81.32	0.81
	40%	9.20x10^{-3}	82.96	0.83	1.79 x10^{-5}	83.11	0.83
	50%	4.80 x10^{-3}	91.11	0.91	6.13 x10^{-6}	94.22	0.94
Seeds extract	2%	0.021	61.11	0.61	4.13 x10^{-5}	61.04	0.61
	5%	0.015	72.22	0.72	3.04 x10^{-5}	71.32	0.71
	10%	0.012	77.78	0.78	2.37 x10^{-5}	77.64	0.78
	15%	9.80 x10^{-3}	81.85	0.82	2.07 x10^{-5}	80.47	0.80
	20%	9.30 x10^{-3}	82.78	0.83	1.86 x10^{-5}	83.11	0.83
	30%	9.02 x10^{-3}	83.30	0.83	1.69 x10^{-5}	84.06	0.84
	40%	6.20 x10^{-3}	88.50	0.89	9.12 x10^{-6}	91.39	0.91

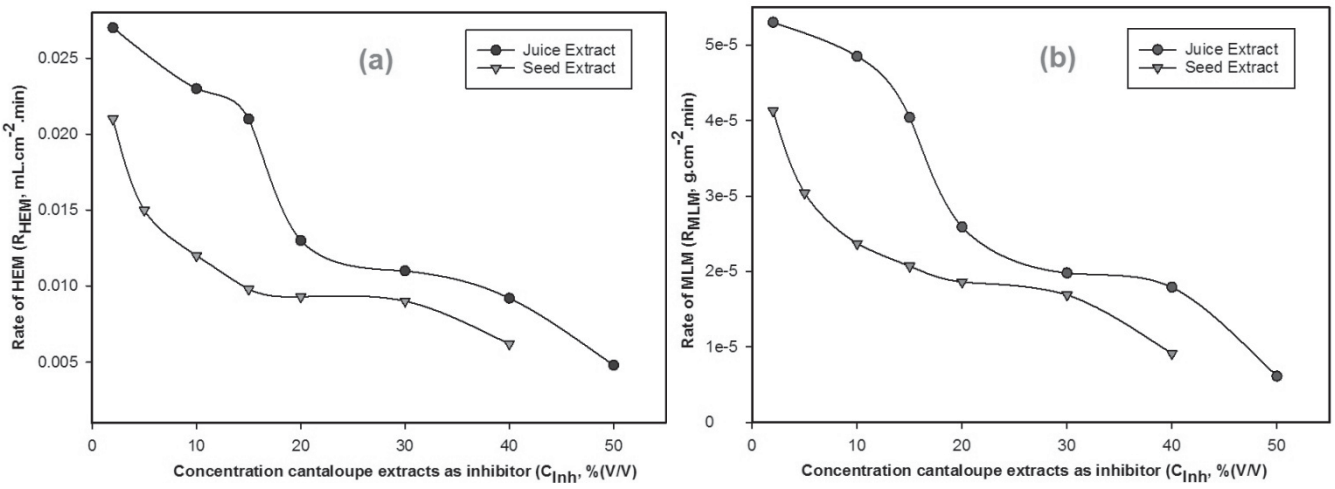

Figure 5. Plots (a) RHEM (b) RMLM via concentrations (%v/v) of cantaloupe extracts in 1.0 M HCl solution at 27°C.

Adsorption isotherm and adsorption parameters

Adsorption isotherms are usually used to describe the adsorption process. The most frequently used isotherms include: Langmuir, Temkin and Flory-Huggins. The adsorption isotherm provides important clues regarding the nature of the metal inhibitor interaction, and inhibitor molecules adsorb on the metal surface if the interaction between molecule and metal surface is higher than that of the H_2O molecule and the metal surface (Shukla and Ebenso, 2011). Langmuir isotherm was tested for its fit to the experimental data according to Equation (16) (Langmuir, 1917; Christov and Popova, 2004).

$$log\ {}^{C}/_{\theta} = -\log K + \log C \quad (16)$$

Where C is the concentration of inhibitor, K is the adsorptive equilibrium constant, θ is the surface coverage.

Langmuir isotherm given band is represented in Figure 7, and listed in Table 6. Where plots of log C/θ versus logC_{inh}, for juice and seed extracts were found straight lines with a good square correlation coefficient (R^2)

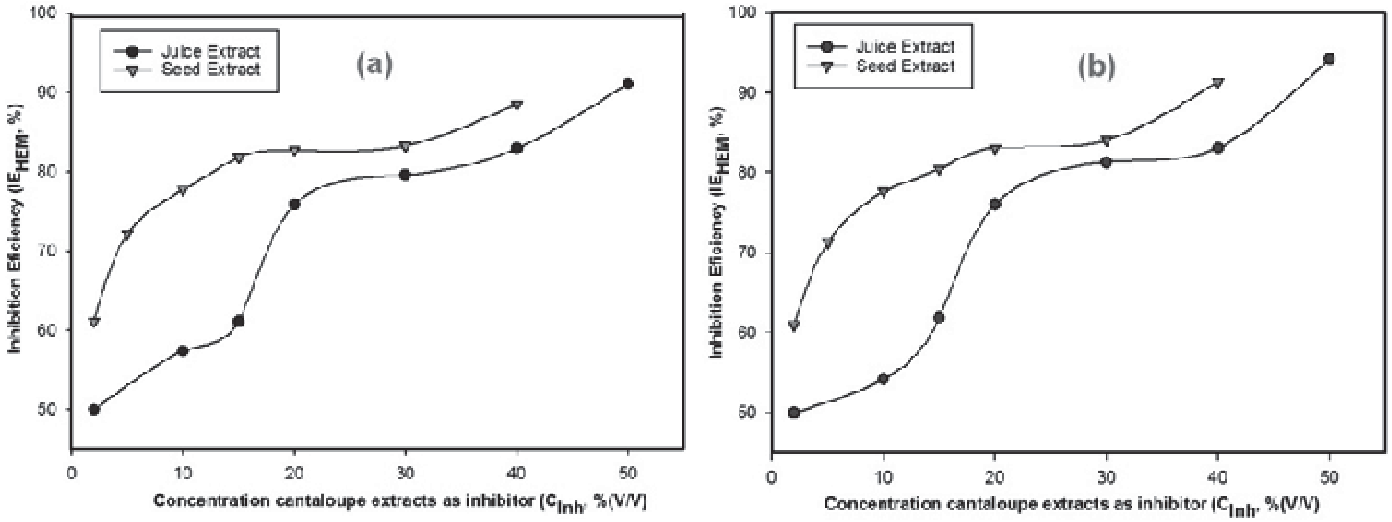

Figure 6. Variations of the inhibition efficiency for (a) HEM (b) MLM with concentrations of inhibitors %(v/v) in 1.0 M HCl solution at 27°C.

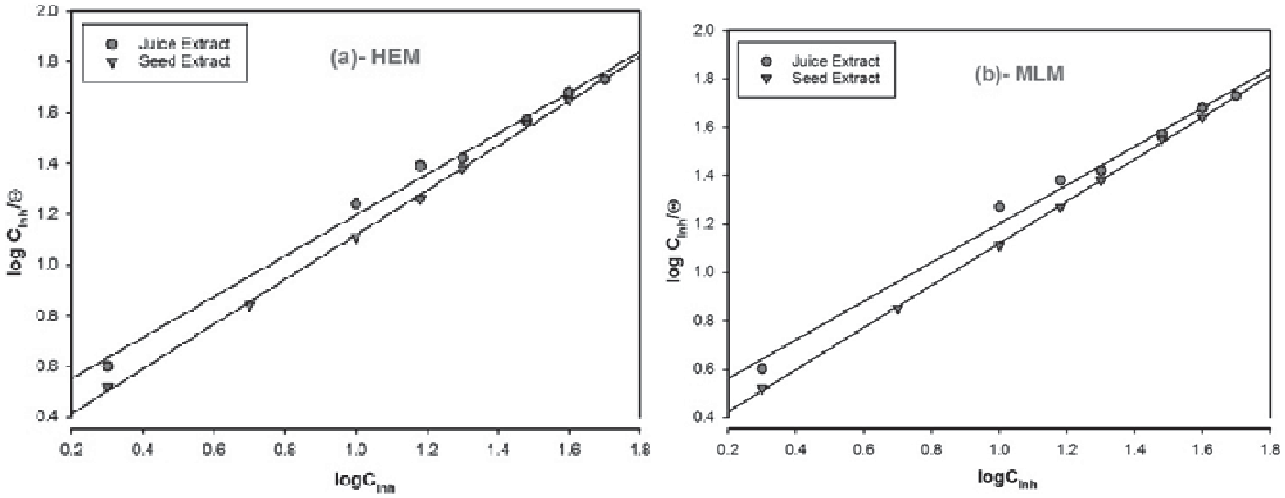

Figure 7. Langmuir adsorption isotherm for cast iron in 1.0M HCl solution of cantaloupe extracts as inhibitors by using (a) HEM (b) MLM at 27°C.

Table 6. Adsorption parameters for adsorption of cantaloupe extracts on cast iron surface under effect 1M HCl solution by using HEM MLM at 27°C.

Isotherm and extracts		HEM			MLM		
		R^2	K		R^2	K	
Langmuir	Juice	0.992	0.41	**slope=** 0.80	0.989	0.40	**Slope=** 0.80
	Seed	0.999	0.58	**slope=** 0.87	0.999	0.56	**slope=** 0.87
Temkin	Juice	0.845	15.48	**a=** -3.90	0.816	11.48	**a=** -3.69
	Seed	0.961	741.31	**a=** -5.80	0.976	416.87	**a=** -5.45
Flory-Huggins	Juice	0.664	4.57	**x=** 1.18	0.576	0.15	**x=** 0.90
	Seed	0.938	2.04	**x=** 2.17	0.895	1.29	**x=** 1.85

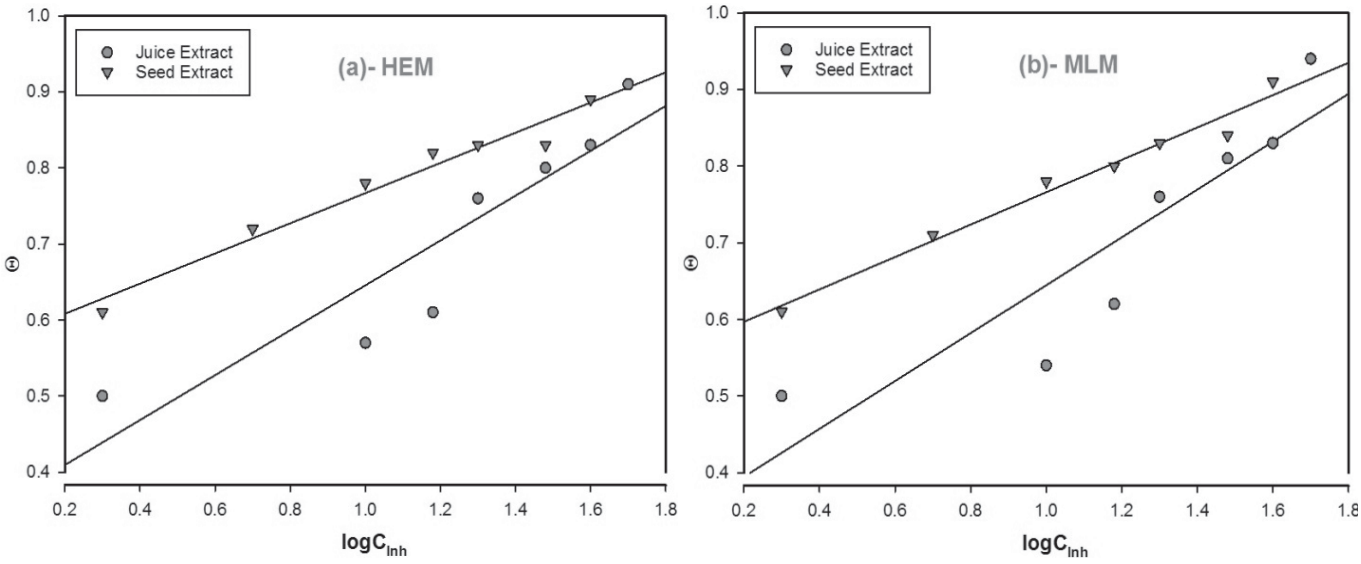

Figure 8. Temkin adsorption isotherm for cast iron in 1.0 M HCl solution of cantaloupe extracts as inhibitors by using (a) HEM (b) MLM at 27°C.

0.992, 0.999 for HEM, and 0.989, 0.999 for MLM, respectively. The slopes lines for each method and extracts are arched unity, it is assumed that the inhibition of cast iron corrosion in 1.0 M HCl by cantaloupe extract occurs by monolayer adsorption at appropriate sites on the metal, the metal surface contains a fixed number of adsorption sites and each site holds one adsorbate, and no interaction between adsorbate molecules. From the intercepts of the straight lines logC/θ axis for juice and seeds extracts, K value calculated were 0.41 and 0.58 $Lmol^{-1}$ for HEM, and 0.40 &0.56 $Lmol^{-1}$ for MLM, respectively. For Temkin adsorption isotherm, the degree of surface by using HEM and MLM is related to logarithmic inhibitor concentration (C) according to (Equ. 17) (Christov and Popova, 2004):

$$\theta = {}^{-2.303}/_{2a}\log K - {}^{2.303}/_{2a}\log C \quad (17)$$

where K is the adsorption equilibrium constant and (a) is the attractive parameter. Plots of θ against log C, as presented in Figure 8 gave linear relationship, which shows that adsorption data fitted Temkin adsorption isotherm at seed extract (R^2= 0.961 and 0.976) for HEM and MLM more than juice (R^2= 0.845 and 0.816) for HEM and MLM, respectively. Adsorption parameters obtained were recorded in Table 6. The values of interaction parameter (a) was negative in all cases, which indicate that repulsion exists in the adsorption layer. Flory-Huggins adsorption isotherm can be expressed according to (Equation 18) (Christov and Popova, 2004):

$$\log ({}^{\theta}/_{C}) = \log K + x\log(1-\theta) \quad (18)$$

Where x is the number of inhibitor molecules occupying one site, or the number of water molecules replaced by one molecule of the inhibitor. The value x substituted by a given inhibitor molecule adsorbed surface by plots of $\log ({}^{\theta}/_{C})$ against $\log(1-\theta)$ by using HEM and MLM, were shown in Figure 9. The values of the size parameter x are positive 1.18 and 2.17 of HEM, 0.90 and 1.85 of MLM for juice and seed cantaloupe extracts, respectively as shown in Table 6. The values of $x \approx 1$ for juice extract, implied that one inhibitor molecule replaces one water molecule, while, the values of $x > 1$ for seeds extract, means that one inhibitor molecule replaces more than one water molecule. *The x* obtained for the seeds extract were higher than those obtained for the juice extract, suggesting that the adsorption behavior of the *seeds extract* is better than that of the juice extract in Flory-Huggins isotherm. According to the fit experimental data (R^2), the better adsorption isotherm of juice and seeds extracts of cantaloupes is Langmuir isotherm.

Conclusion

The results obtained from HEM and MLM of corrosion and corrosion inhibition of cast iron in various concentrations HCl solutions (0.5-2.0 M), under 27°C; can be deduced:

(1). The corrosion rate of cast iron increase with increase concentration of HCl solution.
(2). Juice and seed extracts of cantaloupe acts as good natural inhibitor for corrosion of cast iron in 1.0 M HCl solution.

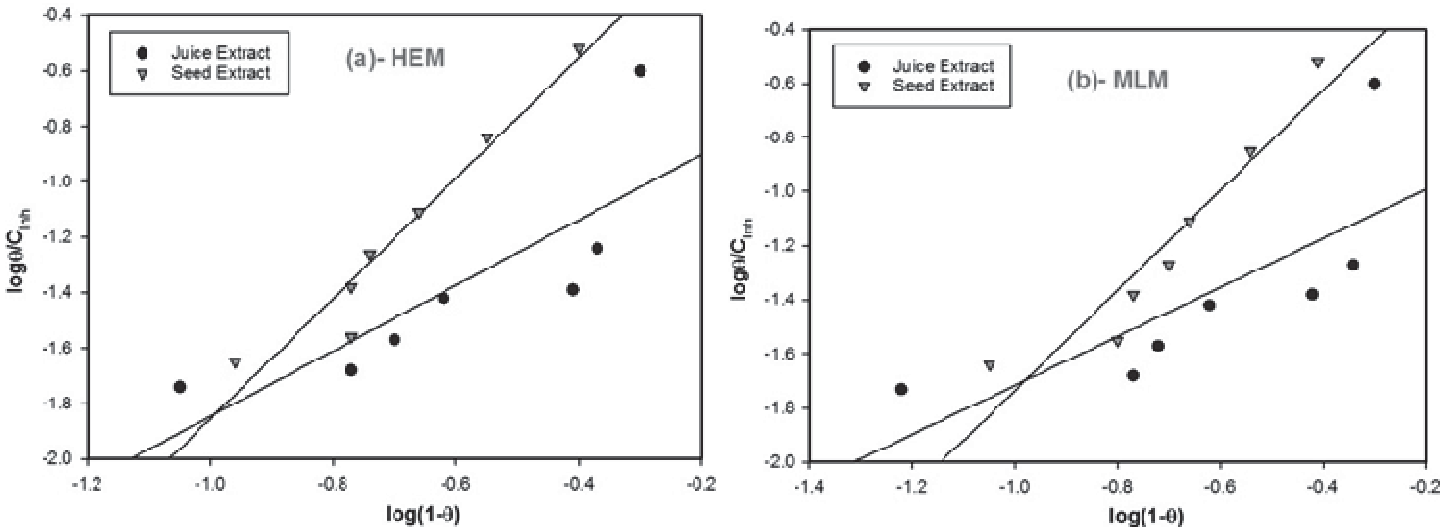

Figure 9. Flory-Huggins adsorption isotherm for cast iron in 1.0M HCl of cantaloupe extracts as inhibitors by using (a) HEM (b) MLM at 27°C.

(3). The inhibition efficiency increase with increase concentration of inhibitors %(v/v), with maximum value obtained in juice extract 91.11 and 94.22 at 50%(v/v), while in seed extract 88.50 and 91.39 at 40%(v/v) for HEM and MLM, respectively.
(4). Seed extract good natural inhibitor than juice extract of cantaloupe.
(5). The square correlation coefficient (R^2) was used to choose the adsorption isotherm that fits experimental data. The adsorption of cantaloupe juice and seed extracts molecules on cast iron surface in 1.0M HCl follows Langmuir adsorption isotherm.

Conflict of Interest

The authors have not declared any conflict of interest.

REFERENCES

Al-Tturkustani A, Arab S, Al-Reheli A (2010). Corrosion and corrosion inhibition of mild steel in H_2SO_4 solutions by zizyphus spina-christi as green inhibitor. Int. J. Chem. 2(2):54-76.
Barouni K, Bazzi L, Salghi R, Mihit M, Hammouti B, Albourine A, El Issami S (2008). Some amino acids as corrosion inhibitors for copper in nitric acid solution. Mater. Lett. 62(19):3325–3327.
Bockris JO, Drazic D (1962). The kinetics of deposition and dissolution of iron: Effect of alloying impurities. Electrochim. Acta. 7(3):293-313.
Bockris JO, Swinkels DA (1964). Adsorption of n-Decylamine on Solid Metal Electrodes. J. Electrochem. Soc. 111(6):736-743.
Bouyanzer A, Hammouti B, Majidi L, Haloui B (2010). Testing Natural Fenugreek as an Ecofriendly Inhibitor for Steel Corrosion in 1 M HCl. Port. Electrochim. Acta. 28(3):165-172.
Branzoi V, Branzoi F, Baibarac M (2000). The inhibition of the corrosion of Armco iron in HCl solutions in the presence of surfactants of the type of ***N***-alkyl quaternary ammonium salts. Mater. Chem. Phys. 65(3):288-297.
Christov M, Popova A (2004). Adsorption characteristics of corrosion inhibition from corrosion rate measurments. Corros. Sci. 46:1613-1620.
Damani M, Et-Touhami A, Al-Deyab SS, Hammouti B, Bouyanzer A (2010). Corrosion inhibition of C38 Steel in 1 M HCl: A comparative study of black pepper extract and its isolated piperine. Int. J. Electrochem. Sci. 5(8):1060-1069.
El-Etre AY (2003). Inhibition of aluminum corrosion using Opuntia extract. Corr. Sci. 45():2485–2495.
Emran K, Ahmed NM, Torjoman BA, Al-Ahmadi AO, Sheekh SN (2014). Cantaloupe extracts as eco friendly corrosion inhibitors for aluminum in acidic and alkaline solutions. J. Mater. Environ. Sci. 5(6):1940-1950
Gadow HS, Fouda AS (2014). *Black tea* as green corrosion inhibitor for carbon steel in 1 M hydrochloric acid solutions. Int. J. Adv. Res. 2(1):233-243.
Gonda I, Bar E, Portnoy V, Lev Sh, Burger J, Schaffer AA, Tadmor Y, Gepstein Sh, Giovannoni JJ, Katzir N, Lewinsohn E (2010). Branched-chain and aromatic amino acid catabolism into aroma volatiles in *Cucumis melo* L. fruit. J. Exp. Bot. 61(4):1111–1123.
Kumar KP, Pillai MS, Thusnavis G (2010). Pericarp of the fruit of *Garcinia Mangostana* as corrosion inhibitor for mild steel in hydrochloric acid medium. Port. Electrochim. Acta. 28(6):373-383.
Lahhit N, Bouyanzer A, Desjobert JM, Hammouti B, Salghi R, Costa J, Jama B, Majidi L (2011). Fennel (*Foeniculum vulgare*) essential oil as green corrosion inhibitor of carbon steel in hydrochloric acid solution. Port. Electrochim. Acta. 29(2):127-138.
Langmuir I (1917).The Constitution and fundamental properties of solids and liquids/liquids. J. Am. Chem. Soc. 39(9):1848–1906.
Mathur PB, Vasudaven T (1982). Reaction Rate studies for the corrosion of metals in Acids-I, Iron in Mineral Acids. Corrosion. 38(3):150-160.
Milind P, Kulwant S (2011). Musk Melon is Eat-Must Melon. IRJP. 2(8):52-57.
Nattaporn W, Pranee A (2011). Effect of pectinase on volatile and functional bioactive compounds in the flesh and placenta of 'Sunlady' cantaloupe. Int. Food Res. J. 18:819-827.
Oguzie EE (2007). Corrosion inhibition of aluminum in acidic and alkaline media by Sansevieria trifasciata extract. Corr. Sci. 49(3):1527-1539.
Popova A, Veleva S, Raicheva S (2005). Kinetic approach to mild steel corrosion. React. Kinet. Catal. L. 85(1):99-105.
Quraishi MA, Yadav DK, Ahamad I (2009). Green approach to corrosion inhibition by black pepper extract in hydrochloric acid

solution. The open Corr. J. 2:56-60.
Shanableh A (2011). Studies on natural extracts as inhibitors of mild steel corrosion in 1M HCl solution. Master thesis, American University of Sharjah, Sharjah, UAE.
Shukla SK, Ebenso E (2011). Corrosion inhibition, adsorption behavior and thermodynamic properties of streptomycin on mild steel in hydrochloric acid medium. Int. J. Electrochem. Sci. 6(8):3277-3291.
Singh AK, Quraishi MA (2012). Study of some Bidentate Schiff Bases of Isatin as corrosion inhibitors for mild steel in hydrochloric acid solution. Int. J. Electrochem. Sci.7:3222–3241.
Rocha JC, Gomes JA, Elia ED, Cruz AP, Cabral LM, Torres AG, Monteiro MV (2012). *Grape Pomace* extracts as green corrosion inhibitors for carbon steel in hydrochloric acid solutions. Int. J. Electrochem. Sci. 7(12):11941-11956.
Zaafarany I (2012). Corrosion inhibition of aluminum in aqueous alkaline solutions by alginate and pectate water-soluble natural polymer anionic polyelectrolytes. Port. Electrochim. Acta. 30(6):419-426.

academicJournals

Vol. 9(3), pp. 50-57, March, 2015
DOI: 10.5897/AJPAC2014.0593
Article Number: A3C12A751546
ISSN 1996 - 0840

http://www.academicjournals.org/AJPAC

African Journal of Pure and Applied Chemistry

Full Length Research Paper

Efficiency enhancement in P3HT:PCBM blends using Squarylium III dye

M. Tembo[1]*, M. O. Munyati[2], S. Hatwaambo[1] and M. Maaza[3]

[1]Department of Physics, School of Natural Sciences, University of Zambia, P. O. Box 32379, Lusaka, 10101 Zambia.
[2]Department of Chemistry, School of Natural Sciences, University of Zambia, P. O. Box 32379, Lusaka, 10101 Zambia.
[3]Nanosciences Laboratories, Materials Research Department, iThemba LABS, P. O. Box 722, Somerset West 7129, Western Cape, South Africa.

Received 24 September, 2014; Accepted 27 January, 2015

Nano-size thin films comprising poly (3-hexylthiophene) (P3HT) and a fullerene derivative [6, 6] phenyl-C_{61}-butyric acid methyl ester (PCBM) incorporating squarylium dye III (SQ3) are reported. The materials prepared were evaluated for their optical, electrical and photo-conversion efficiency. Active layer materials comprising a blend of P3HT:SQ3:PCBM were deposited by spin-coating to produce thin films measuring 100 nm and subsequently annealed at 140°C for 10 min. The films were characterized by UV-Vis-NIR spectroscopy for their optical properties, atomic force microscopy for surface morphology and film thickness, and electrical properties. Optical measurements for blends incorporating different amounts of dye showed increased photo-absorbance with increasing dye concentration. The combined contribution of SQ3 and thermal annealing resulted in increased power conversion efficiency (η) of pristine P3HT:PCBM solar cells from 1.9 to 3.9 %. The dye in the active layer improved photo-absorption by enhanced light harvesting while thermal treatment improved the nanoscale morphology leading to better metal-film interface contact and broadening of the absorption wavelength range.

Key words: Polymer solar cell (PSC), squarylium dye III (SQ3), bulk hetero-junction (BHJ), power conversion efficiency (PCE), poly (3-hexylthiophene (P3HT), [6, 6]-phenyl C_{60} butyric acid methyl ester (PCBM).

INTRODUCTION

Energy is essential to modern society. Its global demand has continued to increase due to increasing population and rapid economic development in Africa. Depletion in fossil fuel resources together with the demand for more environmentally friendly energy sources has given impetus to research on 'green' energy alternatives.

*Corresponding author. Email: mozesio@hotmail.com, Tel: +260 211 231385. Fax: +260 211 238483.

Abbreviations: **BHJ,** Bulk hetero-junction; **HOMO,** Highest occupied molecular orbital; **LUMO,** Lowest unoccupied molecular orbital; **OPVs,** Organic Photovoltaics; **P3HT,** poly (3-hexylthiophene); **PCBM,** [6, 6]-phenyl C_{60} butyric acid methyl ester; **PCE,** Power conversion efficiency; **PEDOT:PSS,** 3, 4-polyethylenedioxythiophene-polystyrenesulfonate; **PSCs,** Polymer Solar Cells; **PV,** Photovoltaic; **QE,** Quantum efficiency; **SQ3,** Squarylium III dye.

Conversion of solar energy via photo-voltaic systems has emerged as one of the most promising of the green energy alternatives that can be deployed on a large scale. The cost of generating power using the current solar cells is more expensive than commercial power generation (Miyake et al., 2010). Conventional solar cells currently are made of silicon which is associated with high manufacturing cost due to processes that requires high temperature and vacuum. Additionally, dissemination has been hampered by high installation costs. Polymer solar cells offer a tantalizing possibility of lower cost devices. One of the most promising polymer solar cell (PSCs) in terms of efficiency and long term stability, is the system based on regio-regular poly(3-hexylthiophene) (rrP3HT) as the electron donor and the fullerene derivative [6,6]-phenyl-C61-butyric acid methyl ester (PCBM) as the electron acceptor material. To attain high efficiencies in PSCs, there is need to understand the fundamental electronic interactions between the polymeric donors and the fullerene acceptors as well as the complex interplay of device architecture, morphology and processing. Additionally, a sound understanding of the fundamental electronic processes involved is important.

The state of the art in the field of PSCs is currently represented by bulk hetero-junction (BHJ) solar cells based on P3HT and PCBM (Yu et al., 1995; Hoppe, 2006; Kim et al., 2006; Ma et al., 2005; Padinger et al., 2003; Reyes-Reyes et al., 2005). Low photo-conversion efficiencies of polymer solar cells compared to their inorganic counter-parts have remained a major drawback towards commercialization. Photo-conversion is typically below 9%. The limitation towards achieving high efficiencies can in-part be attributed to their narrow absorption band which lies in the 450 to 750 nm region. P3HT has a large band gap of about 1.9 eV with a limiting wavelength of harvested light of 650 nm. Almost half of the sun's power spectrum lies outside the absorption range of many organic systems (Bird et al., 1986; Diffey, 1991). Hence, thicker layers in the order of 300 nm would be required to enhance photo-absorption. However, use of layers of this thickness would lead to recombination of charges. As a compromise, polymer layers are typically 200 nm (Stratakis and Kymakis, 2013).

Organic dyes have been used to increase light harvesting capacity in P3HT:PCBM blend (Ameri et al., 2013). Squaraine dyes have been reported as promising small molecules that can be incorporated into polymer solar cells to improve light harvesting capacity owing to their intense absorption in the long wavelength range (Chen et al., 2014). Power conversion efficiencies of 5.5% have been obtained in ternary P3HT:PCBM systems incorporating a squaraine dye following thermal annealing (Rao et al., 2014). They observed enhanced absorption in the range 650 to 780 nm relative to P3HT:PCBM blend. Huang et al. (2013) demonstrated experimentally that in addition to extending absorption in the solar spectrum, small molecules, such squaraine dyes (SQ), improved excit on harvesting via Förster resonance energy transfer (FRET). Inclusion of SQ provides two mechanisms for charge transfer following excitation. The first one involves excitation of P3HT and charge transfer to PCBM while the second is charge transfer involving FRET of the P3HT excitation to SQ and subsequent dissociation. In this paper we report the improvement in power conversion efficiency of pristine P3HT:PCBM through the combined contribution of squarylium III dye (SQ3) and thermal annealing. Ternary P3HT:SQ3:PCBM systems showed an increase in absorption maximum and a red shift in the absorption band. The combined effect of dye inclusion and thermal annealing was to increase power conversion efficiency from 1.9 to 3.9%.

EXPERIMENTAL PROCEDURES

Materials and solutions

Regio-regular P3HT, PCBM and SQ3 were used without further purification. P3HT:PCBM blends containing SQ3 concentrations of 4.76, 9.09, 13.04 and 16.67% were prepared to investigate the effect of dye loading. The blend solutions were vigorously stirred for more than 24 h at room temperature under nitrogen atmosphere in a glove box to maximize mixing.

Film and device fabrication

For optical absorption measurements, the P3HT:PCBM and P3HT:SQ3:PCBM blend films (with different concentrations of the dye) were prepared by spin-coating the solutions onto cleaned micro-glass substrates. Thin film preparation and thermal annealing conditions were kept the same as those of the corresponding devices for accurate comparison. For solar cell fabrication, ITO-glass (15 Ω/ϒ) substrates were sequentially cleaned in an ultrasonic bath using acetone and methanol, rinsed with de-ionized water then finally dried. PEDOT:PSS was spin-coated onto the ITO layer in air and dried using a digitally controlled hot plate at 100˚C for10 minutes. The PEDOT:PSS layer increased the electrode work function and its electrical connection with the organic active layer. The P3HT:PCBM and P3HT:SQ3:PCBM blend solutions were spin-coated (1500 rpm) on top of the insoluble PEDOT:PSS layer. Thin films were then heated at 100℃ for 10 min to removing any residual solvent. A 100 nm thick aluminum (Al) electrode was thermally deposited onto the active layer using a vacuum deposition system at a pressure of about 3 x 10^{-4} Pa through a shadow mask to obtain cells with an active area of 1cm^2. Devices were thermally annealed at 140℃ for 4 min. The complete organic solar cells, with a configuration shown in Figure 1, were stored in the dark under suitable pressure until measurement.

Measurements

Films prepared were characterized for their optical properties using a Lambda 90 UV-Vis-NIR spectrophotometer before and after annealing. Morphological characteristics were established by atomic force microscopy. The power conversion efficiency (PCE) was calculated from the Current-Voltage (I-V) characteristics under

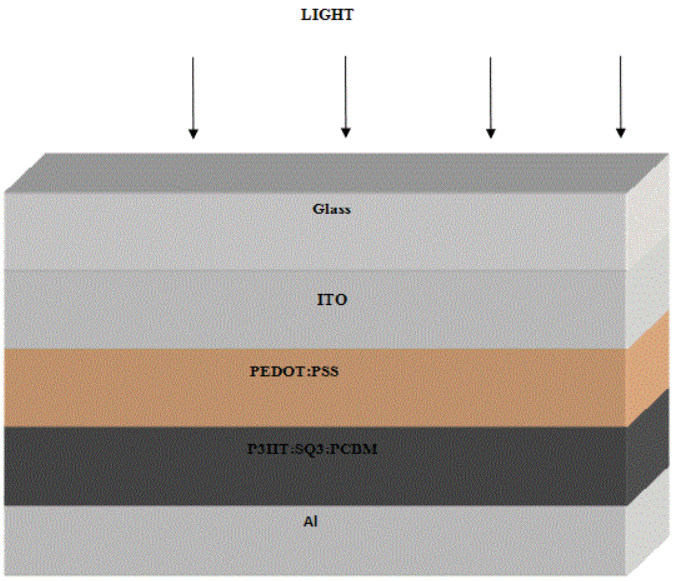

Figure 1. Polymer solar cell configuration showing the different layers of materials.

air mass 1.5 global (1.5 G) solar simulated light irradiation of100 mW/cm^2. Current-voltage characteristics were measured using a KEITHLEY 4200 at room temperature in nitrogen atmosphere.

RESULTS AND DISCUSSION

Absorption characteristics of P3HT:SQ3:PCBM blends

The chemical structures of SQ3 are shown in Figure 2. Absorption spectra of the active layer materials (P3HT, PCBM and SQ3 dye) are shown in Figure 3. It is shown in this figure that PCBM absorbs mainly below the wavelength region of 500 nm. The P3HT spectrum shows an absorption peak at 511nm and absorption edge extending to 630 nm. P3HT also has vibronic shoulders at 547 and 607 nm and these are associated with π-π^* stacking in P3HT and indicative of its crystallinity. SQ3 shows an absorption band extending in the longer wavelength region extending to 650 nm with an absorption peak at 627 nm.

The contribution of SQ3 in light harvesting was investigated by incorporating SQ3 in quantities of 4.76, 9.09, 13.04 and 16.67% in P3HT:PCBM solar cell active layer are shown in Figure 4. Inclusion of SQ3 improves the absorption profile of the P3HT:SQ3:PCBM blend with an increase in absorption intensity and widening the absorption range from the visible to near – infra red. This can be attributed to the combined effect of the P3HT absorption (400 to 700 nm) and SQ3 (550 to 575 nm) spectrum. The shape of the shoulders at about 547 and 607 nm remain relatively the same as SQ3 increased.

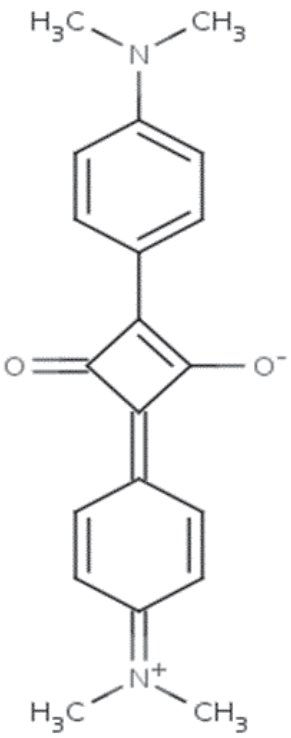

Figure 2. Structure of SQ3 dye .

This indicates that there was no disruption to P3HT crystallinity (Aziz et al., 2014). Increasing the dye content in the P3HT:PCBM blend increases light harvesting through the increase in absorbance and broadening of

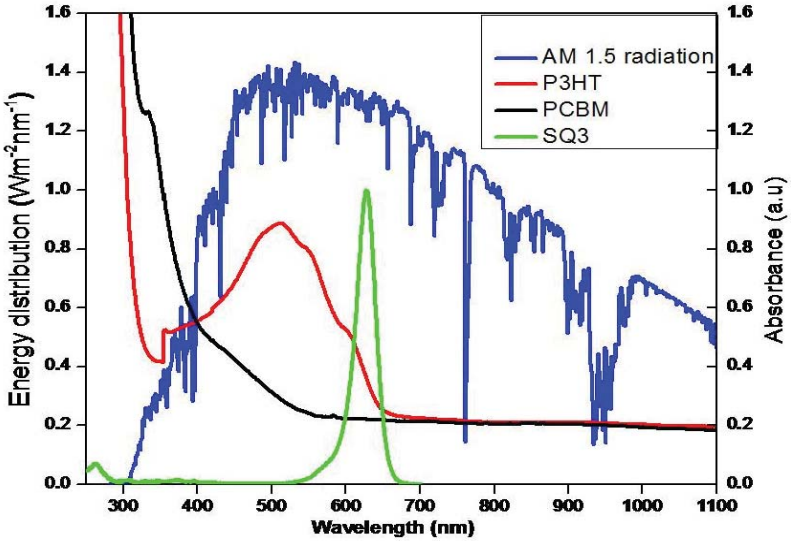

Figure 3. Absorption spectra for spin coated P3HT, PCBM and SQ3 dye thin films compared with the standard AM1.5 solar spectrum.

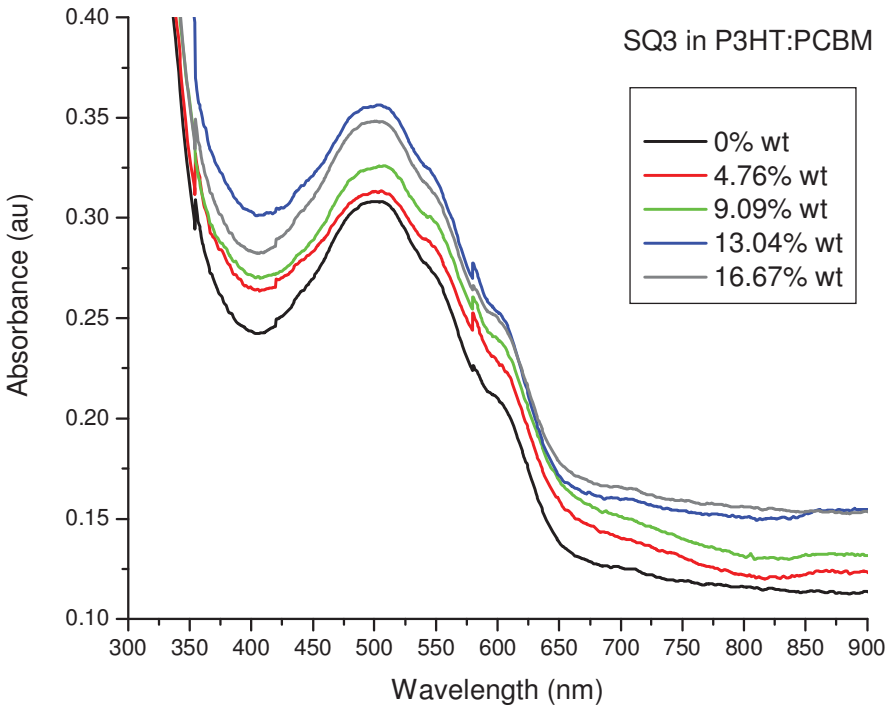

Figure 4. Absorbance spectra of pristine P3HT:SQ3:PCBMwith varying dye loading.

the absorption range. Additionally, the peak absorbance increased from 0.31 to 0.36 a.u representing about 16% increment. Since the absorption at about 600 nm is associated with P3HT crystallinity, an increase would suggest the formation of a more ordered morphology promoted by SQ3 molecules. Thus, the total number of photons absorbed by the solar cell active layer increases when SQ3 dye is added to the P3HT:PCBM blend. The increase is due to a synergistic effect in the absorption characteristics of P3HT and SQ3. However, there is a decrease in absorbance when the concentration of SQ3 was 16.67%. The decrease may be attributed to the

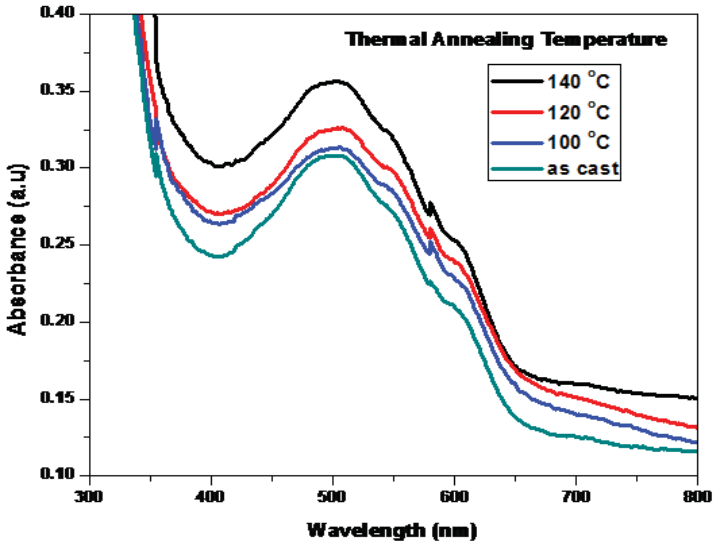

Figure 5. UV-Vis absorbance spectra of 100 nm P3HT:PCBM blend films spin coated at 1400 rpm treated in the following ways: as cast (green), thermally annealed at 100°C (blue), 120 ˚C (red) and 140°C.

disturbed interpenetrating network between P3HT and PCBM with the relative decrease in the P3HT:PCBM content with the high concentration of SQ3, which hinders the charge transportation (An et al., 2014; Cha et al., 2013; Rao et al., 2014).

Effect of annealing

UV-Vis absorption spectroscopy was used to study the effect of thermal annealing on thin films of P3HT:PCBM spin coated on glass substrates. Thermal annealing optimized the morphology of P3HT:PCBM thin films and thus improved photo-absorbance as shown in Figure 5. The untreated film has peak absorbance of 0.30 a.u. and shoulders at 501, 545 and 597 nm. Thermal annealing at temperatures of 100, 120 and 140°C increased the peak absorbance to 0.31, 0.32 and 0.36 a.u respectively. The increase in absorption intensity is associated with higher crystallinity of P3HT following reordering in annealed samples. Additionally, films treated at 140°C show a red shift of peak absorption wavelength from 501 to 510 nm while the shoulders shift to 549 and 604 nm respectively. The red shift is ascribed to increased inter-chain interaction among the P3HT chains arising from annealing. This results in lowering of the band gap and increase in of the optical π-π^* transition, an indication of formation of crystallites.

Atomic Force Microscope (AFM) studies

AFM was used to evaluate the effect of adding SQ3 and thermal annealing on P3HT: PCBM blends. The images are shown in Figure 6. The results show that as cast films without SQ3 had a surface roughness of 0.38 nm while samples annealed at 140°C had a roughness of 0.75 nm. A significant increase in roughness was observed on addition of SQ3 weight of 13.04%. However, annealing at140°C of P3HT:SQ3:PCBM showed a slight decrease in roughness to 0.8 nm. An increase in roughness is associated with increased order in the P3HT phase (Aziz et al., 2014). Thus, the slight reduction suggests reduced crystallinity and disturbance in the morphology at a dye load of 6 mg and annealing temperature of 140°C. Huang et al. (2013) showed that SQ molecules was prefer to reside at the interface between P3HT and PCBM increasing phase separation in the polymer blend. Decrease in roughness maybe a result of loss of the favoured morphology following annealing at 140°C.

Electrical properties

The solar cell electrical characteristics are determined by measuring the current density to voltage (I-V) characteristics, both in dark and under illumination. The open circuit voltage (V_{oc}), short circuit current (I_{sc}), fill factor (FF) and maximum power point (P_{max}) were deduced from the I-V curve. The power conversion efficiency is subsequently determined using these data and is tabulated in Table 3.

Current -voltage (I-V) characterization

The polymer solar cell device structure is shown in Table 2 and their I-V curves in Figure 7. The active layer

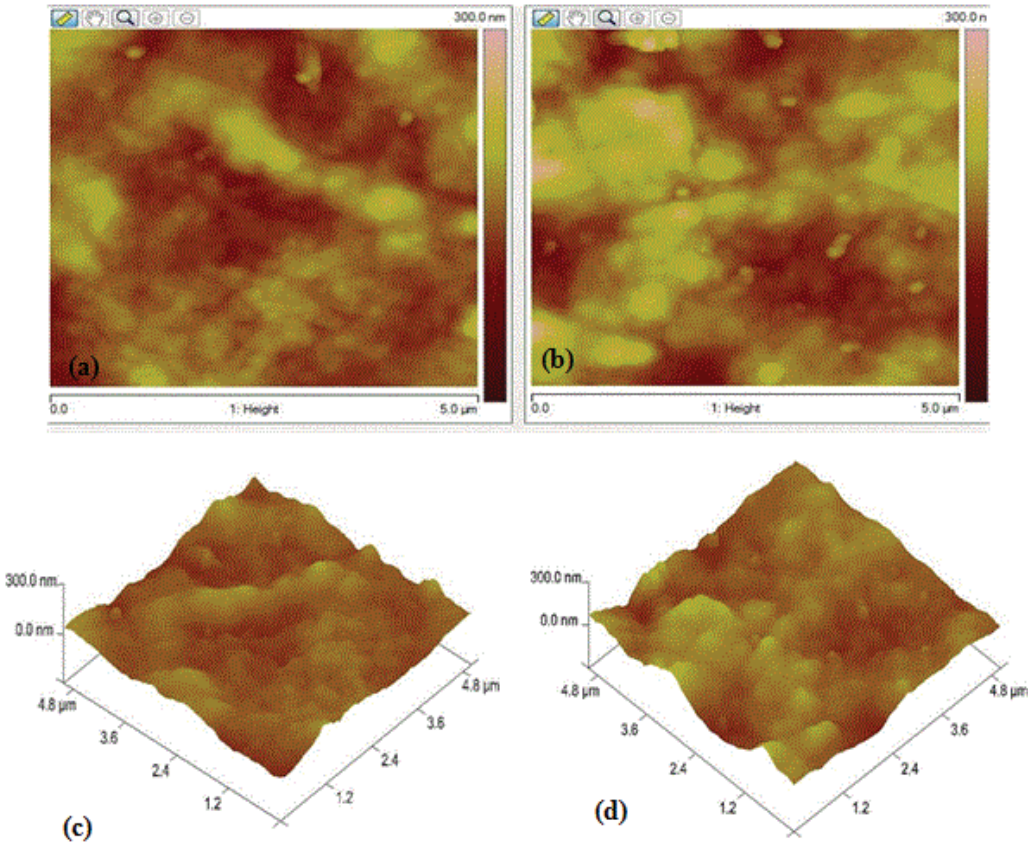

Figure 6. Two dimensional AFM images of P3HT:PCBM (a) and PCBM:SQ3:PCBM (b), 3 Dimension AFM images of P3HT:PCBM (c) and PCBM:SQ3:PCBM (d).

Table 1. Weight percentage of SQ3 in P3HT:PCBM.

SQ3 mass (mg)	PCBM mass (mg)	P3HT mass (mg)	SQ3 weight (%)
2	20	20	4.76
4	20	20	9.09
6	20	20	13.04
8	20	20	16.67

Table 2. Polymer solar cells device structure.

Solar Cell	Device Structure	Illumination	Annealing
A	ITO/PEDOT:PSS/P3HT:SQ3:PCBM/Al	NO	NO
B	ITO/PEDOT:PSS/P3HT:PCBM/Al	YES	NO
C	ITO/PEDOT:PSS/P3HT:SQ3:PCBM/Al	YES	NO
D	ITO/PEDOT:PSS/P3HT:PCBM/Al	YES	YES
E	ITO/PEDOT:PSS/P3HT:SQ3:PCBM/Al	YES	YES

consisted of an active layer of 13.04% weight SQ3 inP3HT:PCBM. Thermal annealing was done at a temperature of 140°C as the optimum temperature. The electrical parameters determined from Figure 7 of the devices and are summarized in Table 3. The control device comprising P3HT:PCBM without SQ3 with no

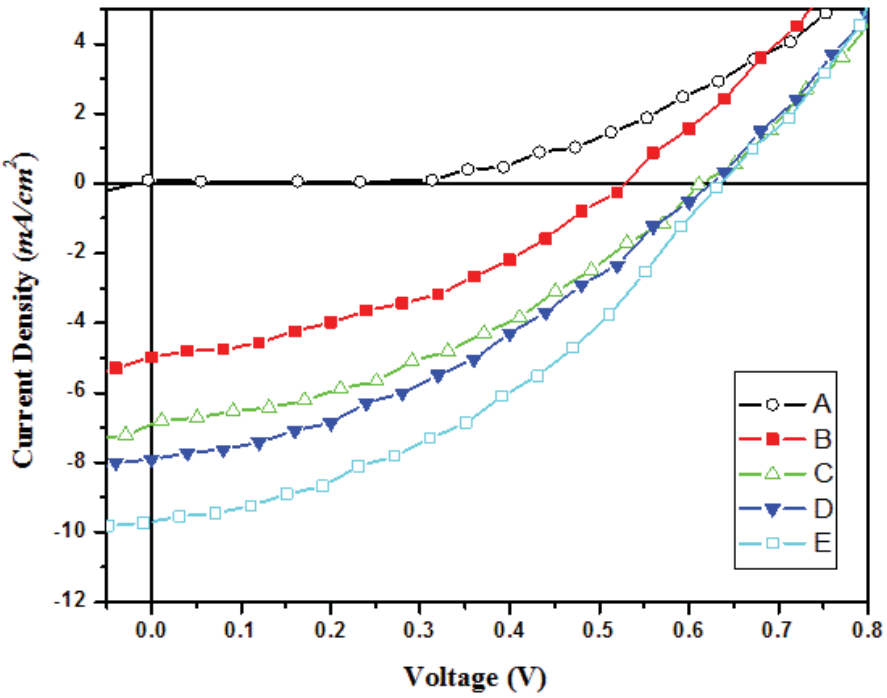

Figure 7. Current versus voltage (I-V) curves obtained for solar cells under AM 1.5 solar spectrum simulations (light) at irradiation intensity of 100 mW.cm^{-2}.

Table 3. Electrical characteristics of P3HT:SQ3:PCBM solar cells.

Solar Cell	V_{oc} (V)	I_{sc} (mA)	I_{max} (mA)	P_{max}	FF	η (%)
B	0.53	5.78	3.39	1.08	0.35	1.3
C	0.61	6.88	4.29	1.59	0.38	2.5
D	0.62	7.88	5.04	1.81	0.37	2.8
E	0.64	9.68	6.86	2.41	0.40	3.9

thermal treatment had a I_{sc} value of 5.7 mA, V_{oc} of 0.32 V and FF of 0.55. The power conversion efficiency (PCE) was established to be 1.3%. The inclusion of SQ3 combined with thermal annealing resulted in a device with 3.9% PCE. The I_{sc} increased from 5.78 mA for the control to 9.68 mA for the annealed ternary blend. The V_{oc} and FF increased from 0.53 to 0.64 mA respectively. Increase in I_{sc} is due to the increase in photo generated excitons arising from the broadened absorption range to the NIR. The V_{oc} is related to the energy difference between the donor HOMO and acceptor LUMO, a change is expected if exciton separation occurs at the donor-acceptor interface. It has been reported by Huang et al. (2013) that the highest occupied molecular orbital (HOMO) of SQ is located in-between the HOMOs of P3HT and PCBM, similarly for the lowest unoccupied molecular orbital (LUMO) levels. Consequently the initial excitation leads to two possible routes for current generation: (i) photo induced charge transfer between P3HT and PCBM, (ii) FRET excitation of P3HT to SQ3 followed by charge dissociation. Thus, increase in PCE from 1.3 to 3.9% can be attributed to the synergistic effect arising from the change in absorption profile to near infra red (NIR) and establishment of an addition charge transfer route in the system. This represents a two-fold increase in PCE.

Conclusion

In this work, we have investigated the effect of adding SQ3 dye to P3HT:PCBM forming a ternary system. The light harvesting capacity was increased by broadening the absorption band to NIR. A red shift was observed with vibronic shoulders shifting from 501 and 547 nm to 510 and 600 nm respectively. The increase in absorption

intensity of these shoulders suggest an increase in P3HT crystallinity. Furthermore, inclusion of SQ3 resulted in broadening of the absorption spectrum. A similar effect was observed as a result of thermal treatment of the ternary system at 140°C.The combined contribution of SQ3 and thermal annealing resulted in increased power conversion efficiency (η) of pristine P3HT:PCBM solar cell from 1.9 to 3.9%. Increase in PCE is attributed to the extension of the absorption range thus improving light harvesting capacity and introduction of an additional charge transfer mechanism through SQ3.

Conflict of Interest

The authors have not declared any conflict of interest.

ACKNOWLEDGMENTS

The authors would like to express gratitude for the financial support from the International Science Program (ISP). Support from Nanoscience Africa Network (NANOAFNAC) and Materials Science and Solar Energy Network for Eastern and Southern Africa (MSSEESA) is duly acknowledged. Special mention should also be made to iThemba LABS, Physics Department of University of Western Cape in South Africa and Physics Department of the University of Dar-es-salaam in Tanzania.

REFERENCES

An Q, Zhang FJ, Li L, Wang J, Zhang J, Zhou L, TangW (2014).Improved efficiency of bulk heterojunction polymer solar cells by doping low-bandgap small molecule. ASC Appl. Interfaces. 6:6537-6544.

Ameri T, Khoram P, Min J, Brabec CJ (2013). Organic Solar Cells: A Review. Adv. Mater. 25:4245-4266.

Aziz F, Ismail FA, Soga T (2014). Effect of solvent annealing on crystallanity of spray coated ternary blend films prepared using low boiling point solvent. Chem. Eng. Process. 79:48-55.

Bird RE, Riordan C (1986).Simple solar spectral model for direct and diffuse irradiance on horizontal and tilted planes at the earth's surface for cloudless atmospheres. J. Climate Appl. Meteorol. 25:87-97.

Cha H, Chung DS, Bae SY, Lee M, An TK, Hwang J, Kim KH, Kim YH, Choi DH, Park CE (2013). Complementary Absorbing Star-Shaped Small Molecules for the Preparation of Ternary Cascade Energy Structures in Organic Photovoltaic Cells. Adv. Funct. Mater. 23(12): 1556-1565.

Chen G, Sasabe H, Wang XF, Hong Z, Kido J (2014). A squaraine dye as molecular snsitizer for increasing light harvesting in polymer solar cells. Synthetic Metals. 192:10-14.

Diffey BL (1991). Solar ultraviolet radiation effects on biological systems. Rev. Phys. Medicine Biol. 36(3):299-328.

Hoppe H, Sariciftci NS (2006).Morphology of polymer/fullerene bulk heterojunction solar cells. J. Mater. Chem. 16:48–58.

Huang JS, Goh T, Li X, Sfeir MY, Bielinsk EA (2013). Improving performance of P3HT/PCBM with squarianedye.In Z. H. Kafafi (Ed.), Organic Photovoltaics XIV, 8830.

Kim JY, Kim SH, Lee H, Lee K, Ma W, Gong X, Heeger AJ (2006). New architecture for high-efficiency polymer photovoltaic cells using solution - based titanium oxide as an optical spacer. Adv. Mater. 18: 572–576.

Ma W, Yang C, Gong X, Lee K, Heeger AJ (2005). Thermally stable, efficient polymer solar cells with nanoscale control of the interpenetrating network morphology. Adv. Funct. Mater.15:1617–1622.

Miyake K, Uetani Y, Seike T, Kato T, Oya K (2010). Development of Next Generation Organic Solar Cell. Sumitomo Chemical Co. Ltd.

Padinger F, Rittberger RS, Sariciftci NS (2003). Effects of postproduction treatment on plastic solar cells. Adv. Funct. Mater. 13: 85-88.

Rao AB, Kumar SM, Sivakumar G, Singh SP, Bhanuprakash K (2014). Effect of incorporation of squaraine dye on the photovoltaic response of buli heterojunction solar cells based on P3HT:PC70BM blend. ACS Sustainable Chem. Eng. 2:1743-1751.

Reyes-Reyes K, Kim D, Carroll L (2005). “High-efficiency photovoltaic devices based on annealed poly(3-hexylthiophene and 1-(3-methoxycarbonyl)-propyl-1-phenyl-(6,6) C61 blends.” Appl. Phys. Lett.87, 083506.

Stratakis E, Kymakis E (2013). Nanoparticle based Plasmonic photovoltaic devices. Materials Today 16(4):133–146.

Yu G, Gao J, Hummelen JC, Wudl F, Heeger AJ (1995). Polymer photovoltaic cells: Enhanced efficiencies via a network of internal donor–acceptor heterojunctions. Science. 270:1789–1791.

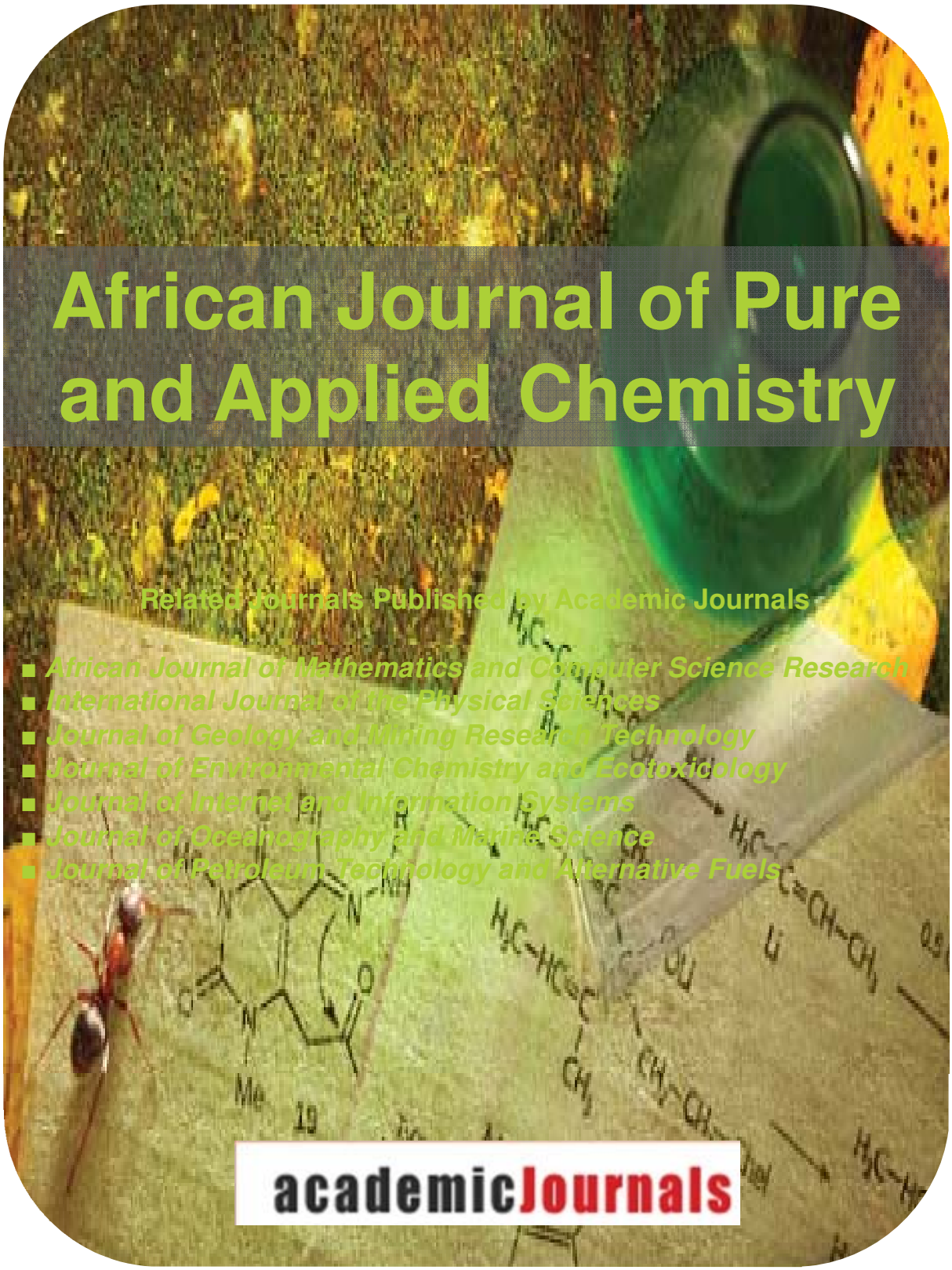

African Journal of Pure and Applied Chemistry

Related Journals Published by Academic Journals

- African Journal of Mathematics and Computer Science Research
- International Journal of the Physical Sciences
- Journal of Geology and Mining Research Technology
- Journal of Environmental Chemistry and Ecotoxicology
- Journal of Internet and Information Systems
- Journal of Oceanography and Marine Science
- Journal of Petroleum Technology and Alternative Fuels

academicJournals